

**Key Points:**

- An inhaled one-micron diameter olivine particle is predicted to dissolve in approximately 24 years inside the human lungs
- Inhaled olivine could react with lung fluid over time and precipitate amorphous silica, ferrihydrite, and asbestos-like minerals
- Inhaled lunar dust could potentially lead to long-term health consequences due to mineral dissolution and precipitation of secondary mineral phases

**Supporting Information:**

Supporting Information may be found in the online version of this article.

**Correspondence to:**

D. A. Hendrix,  
[donald.hendrix@stonybrook.edu](mailto:donald.hendrix@stonybrook.edu)

**Citation:**

Hendrix, D. A., Hurowitz, J. A., Glotch, T. D., & Schoonen, M. A. A. (2021). Olivine dissolution in simulated lung and gastric fluid as an analog to the behavior of lunar particulate matter inside the human respiratory and gastrointestinal systems. *GeoHealth*, 5, e2021GH000491. <https://doi.org/10.1029/2021GH000491>

Received 27 JUL 2021

Accepted 30 OCT 2021

**Author Contributions:**

**Formal analysis:** Donald A. Hendrix, Joel A. Hurowitz, Timothy D. Glotch, Martin A. A. Schoonen





**Funding acquisition:** Joel A. Hurowitz, Timothy D. Glotch

**Investigation:** Donald A. Hendrix

**Methodology:** Donald A. Hendrix, Timothy D. Glotch

© 2021 The Authors. GeoHealth published by Wiley Periodicals LLC on behalf of American Geophysical Union. This is an open access article under the terms of the [Creative Commons Attribution-NonCommercial-NoDerivs License](#), which permits use and distribution in any medium, provided the original work is properly cited, the use is non-commercial and no modifications or adaptations are made.

# Olivine Dissolution in Simulated Lung and Gastric Fluid as an Analog to the Behavior of Lunar Particulate Matter Inside the Human Respiratory and Gastrointestinal Systems

Donald A. Hendrix<sup>1</sup> , Joel A. Hurowitz<sup>1</sup> , Timothy D. Glotch<sup>1</sup> , and Martin A. A. Schoonen<sup>2</sup> 

<sup>1</sup>Department of Geosciences, Stony Brook University, Stony Brook, NY, USA, <sup>2</sup>Environment, Biology, Nuclear Science, & Nonproliferation, Brookhaven National Laboratory, Upton, NY, USA

**Abstract** With the Artemis III mission scheduled to land humans on the Moon in 2025, work must be done to understand the hazards lunar dust inhalation would pose to humans. In this study, San Carlos olivine was used as an analog of lunar olivine, a common component of lunar dust. Olivine was dissolved in a flow-through apparatus in both simulated lung fluid and 0.1 M HCl (simulated gastric fluid) over a period of approximately 2 weeks at physiological temperature, 37°C. Effluent samples were collected periodically and analyzed for pH, iron, silicon, and magnesium ion concentrations. The dissolution rate data derived from our measurements allow us to estimate that an inhaled 1.0 μm diameter olivine particle would take approximately 24 years to dissolve in the human lungs and approximately 3 weeks to dissolve in gastric fluid. Results revealed that inhaled olivine particles may generate the toxic chemical, hydroxyl radical, for up to 5–6 days in lung fluid. Olivine dissolved in 0.1 M HCl for 2 weeks transformed to an amorphous silica-rich solid plus the ferric iron oxy-hydroxide ferrihydrite. Olivine dissolved in simulated lung fluid shows no detectable change in composition or crystallinity. Equilibrium thermodynamic models indicate that olivine in the human lungs can precipitate secondary minerals with fibrous crystal structures that have the potential to induce detrimental health effects similar to asbestos exposure. Our work indicates that inhaled lunar dust containing olivine can settle in the human lungs for years and could induce long-term potential health effects like that of silicosis.

**Plain Language Summary** It is important to understand the long-term consequences of lunar dust inhalation to prepare for the upcoming Artemis mission, the first lunar mission in over 50 years. We measured the dissolution time of a micrometer diameter inhaled olivine particle, a common mineral found in lunar dust, at approximately 24 years. As a result, any particles that are not able to be expelled by the human respiratory system will remain present for many years. Spectroscopic measurements and geochemical models indicate the potential for inhaled olivine to dissolve and then precipitate secondary mineral phases including but not limited to amorphous silica, ferrihydrite, and asbestos-like minerals. These minerals can then remain in the human lungs for longer than the typical human lifespan. Olivine was observed to generate reactive oxidizing compounds in simulated lung fluid which indicates the ability for olivine to induce potential short-term damage upon contact with human lung fluid. Our work highlights the ability of lunar dust, which contains olivine, to induce both potential short- and long-term health effects. This work also highlights the importance in investigating not only the effects of lunar dust on humans but also the need for the continued development of lunar dust mitigation technologies.

## 1. Introduction

### 1.1. Lunar Dust Reactivity, Toxicity, and Exposure Limits—A Brief Review

Artemis and other future lunar missions, which aim to put humans back on the Moon from 2025 onward, will present several major challenges (Crane, 2019). One of the challenges is to keep human explorers healthy as they explore the lunar surface environment. The lunar surface is covered in a layer consisting of particles with an average grain size of 45–100 μm termed the “regolith.” This layer covers approximately the

**Project Administration:** Joel A. Hurowitz, Timothy D. Glotch  
**Writing – original draft:** Donald A. Hendrix  
**Writing – review & editing:** Joel A. Hurowitz, Martin A. A. Schoonen

upper 10 m of the entire lunar surface. Approximately 20% of these particles are less than 20  $\mu\text{m}$ , the fraction informally termed lunar “dust.” Inhalation exposure of lunar dust is recognized as a risk to astronaut health and safety. Most lunar dust is small enough to be inhaled and collected inside the human lungs. The generation of reactive oxygen species (ROS) such as hydroxyl radicals ( $\text{OH}^*$ ) via lunar dust is problematic considering that inhalation of lunar dust rich in minerals such as pyroxene and olivine would lead to tissue and cell damage induced in part by ROS (Caston et al., 2018; Fubini & Hubbard, 2003; Gilmour et al., 1995; Hendrix et al., 2019; Linnarsson et al., 2012; Schoonen et al., 2006). Some Apollo astronauts reported that lunar dust was a nuisance, smelled like gunpowder, and induced allergy-like responses that were described as comparable to hay fever (Scully & Meyers, 2015). To mitigate against these allergic responses, astronauts would sleep with their helmets on to avoid dust exposure (Scully & Meyers, 2015). Lunar Extravehicular Activities (EVA) ranged from a total time of approximately 2 hr to a little over 20 hr for each Apollo mission with total lunar stays between 1 and 4 days (Portree, 1997). Future missions are expected to last weeks and months on the lunar surface and, therefore, total EVA times for each mission would be much longer, putting humans at increased health risks relative to those experienced by the Apollo astronauts. There have been numerous studies performed in an attempt to further understand lunar dust effects on future human explorers by the Lunar Airborne Dust Toxicity Assessment Group (LADTAG) team, the Solar System Exploration Research Virtual Institute (SSERVI), the Remote In Situ and Synchrotron Studies for Science and Exploration (RIS<sup>4</sup>E) Theme 3 group, and others (Caston et al., 2018; Hendrix et al., 2019; Hurowitz et al., 2007; Kaur et al., 2016; Lam et al., 2013; Li et al., 2019; Linnarsson et al., 2012; Loftus et al., 2010; McKay et al., 2015; Meyers et al., 2012; Park et al., 2008; Scully & Meyers, 2015; Turci et al., 2015; Wallace et al., 2009, 2010). Work performed by the LADTAG team resulted in the formulation of a Safe Exposure Estimate (SEE) for lunar dust of  $0.3 \text{ mg m}^{-3}$  during intermittent exposure over a 6-month lunar surface mission (James et al., 2014). Some Apollo missions fared better than others in regard to the efficacy of the lunar dust filtration systems. While it is reasonable to assume that dust filters on board the Artemis III mission will be superior compared to those used on the Apollo mission, it is still important to study the underlying mechanisms of lunar dust toxicity to better prepare medical experts and astronauts in case of accidental lunar dust exposure.

Previous studies have shown that lunar dust is significantly more reactive, as measured by the concentration of hydroxyl radical ( $\text{OH}^*$ ) generated in a regolith-liquid slurry, than most fine-grained terrestrial rock and mineral dusts. For example, Wallace et al. (2009, 2010) determined that lunar dust samples from Apollo 15, 16, and 17 are significantly more reactive relative to the lunar analog regolith, JSC-1A, and the mineral quartz. This study indicated that the presence of iron, particularly nanophase metallic iron (np-Fe), led to large observed increases in reactivity. Notably, soils from mare regions of the lunar surface exhibit greater reactivity than soils from highland regions, even when the two have similar metallic iron content (Wallace et al., 2010). Highland soils contain lower levels of ferrous iron relative to mare soils which possibly indicates that reactivity is both dependent on ferrous iron and metallic iron content. A limited suite of 8 Apollo 15, 16, and 17 samples were used in their study due to the difficulty in obtaining a large, diverse collection of pristine lunar dust samples.

Future missions to the lunar surface, such as Artemis, are planning to land in the South Pole-Aitken Basin, which has lunar materials that have distinct characteristics from the Apollo soils due to a high concentration of volatiles, possibly leading to different toxicological properties that may require modification of exposure limits established by NASA (Colaprete et al., 2010). The use of lunar simulants represents an attempt to address the problem of a lack of lunar dust availability. Using JSC-1A, for example (Turci et al., 2015), determined that  $\text{OH}^*$  generation is due to transition metal ions on the surface of the lunar simulant. Kaur et al. (2016) tested the reactivity of a variety of lunar simulants including JSC-1A, Colorado School of Mines-Colorado Lava (CSM-CL), and Olivine-Bytownite-1 (OB-1) simulants and determined that  $\text{OH}^*$  generation persists even when the process of mechanical pulverization to a fine, respirable powder occurs in an inert atmosphere, implying that  $\text{O}_2$  from the air does not play an important role in the surface reactivity of pulverized minerals. The OB-1 lunar highland simulant was found to generate less  $\text{OH}^*$  relative to the lunar mare simulants JSC-1A and CSM-CL, similar to the results from Wallace et al. (2009), which demonstrated that lunar highland material was less reactive than lunar mare material. There are still caveats to using lunar simulants despite the significantly lower cost and ease of access. Simulants contain terrestrial minerals that do not reflect the chemistry of lunar minerals and they do not contain the metallic

iron present in lunar soils. Lunar simulants are composed of a variety of minerals, so it is not possible to unambiguously determine which constituents of lunar soils enhance reactivity and which do not. In an attempt to determine which mineral constituents of lunar simulants generate the most and least OH\*, Hendrix et al. (2019) studied the OH\* generation potential of olivine, augite, diopside, bytownite, albite, labradorite, and quartz (as a control). Quartz was almost inert and generated the least amount of OH\* relative to all other samples, in accord with the results of Wallace et al. (2009). Fe-rich silicates (i.e., olivine, augite, and diopside) are significantly more reactive relative to Fe-poor silicates (i.e., bytownite, labradorite, albite, and quartz). These findings reflect why lunar simulants such as OB-1 (rich in Fe-poor silicates) are less reactive relative to JSC-1A and CSM-CL (rich in Fe-rich silicates). It should be noted that OH\* generation is only one aspect of dust toxicity and that there is not always a correlation between toxic responses in cells and the capacity for a substance to generate OH\* in solution (Caston et al., 2018). Particle morphology, size, chemical composition, and surface features/defects all can simultaneously contribute to observed toxic responses. Even though OH\* is considered a secondary pathway to observed lunar dust toxicities, it should however be noted that OH\* is a highly reactive chemical species that is capable of oxidizing DNA (Angelé-Martínez et al., 2014; Dizdaroglu et al., 1991; James et al., 2014; Pryor, 1988; Von Sonntag, 1991). Due to the fact that OH\* still is evidenced to induce potential bodily harm, this study assessed the capacity for olivine to generate OH\* for seven days post incubation in both 0.1 M HCl and simulated lung fluid (SLF).

In an effort to step beyond ROS generation assays and directly assess potential toxicity (Caston et al., 2018) and Li et al. (2019) demonstrated that exposure to lunar simulants induces inflammatory responses, cell apoptosis, and damages DNA. Quartz induced the largest inflammatory response and DNA damage relative to the other lunar simulants, similar to the results of James et al. (2013). Li et al. (2019) determined that lunar simulants can induce moderate cytotoxicity in macrophages and alter cell morphology. It is important to assess the impact inhaled lunar dust will have on macrophages since they are one of the first lines of defense against inhaled particulates. Li et al. (2019) found quartz and agglutinated JSC-1A exposure resulted in highly diminished macrophage viability, and indicates the severity of lunar dust exposure, which is known to be largely composed of agglutinates. Macrophages exposed to simulants exhibited a foamy shape, which closely resembles observations of human silicosis and silica-induced lung damage in animal models (Li et al., 2019; Sato et al., 2006).

Pulmonary tests were performed on rats using Apollo 14 soil sample 14003, 96 from the Fra Mauro formation which had been sealed for 38 years before opening, lunar soil simulants, quartz, and the nuisance dust anatase (TiO<sub>2</sub>). James et al. (2013) analyzed the effects of exposing rats via intratracheal installation (ITI) to 0, 1, 2.5, and 7.5 mg of lunar dust in a saline solution. Toxicity markers were analyzed one week and one month after exposure and the results suggested that lunar dust is significantly more toxic than TiO<sub>2</sub> but less toxic than quartz. It was concluded in the study that Permissible Exposure Limits (PEL's) should be set between 0.5 and 1.0 mg m<sup>-3</sup> for extended mission durations up to six months. There were, however, limitations in using the ITI method as the amount of sample required to be injected is far greater than any amounts of lunar dust that would be naturally inhaled, and the dispersion of a fluid-dust slurry is physically different compared to inhalation of dust. Lam et al. (2013) attempted to better replicate human exposure to lunar dust and so conducted an inhalation study using rats. Rats were exposed to 0, 2.1, 6.8, 20.8, and 60.6 mg m<sup>-3</sup> of lunar dust for a period of 4 weeks (6 hr/day, 5 days/week) then euthanized 1 day, 1 week, 4 weeks, and 13 weeks after the last exposure. Exposure to 0, 2.1, and 6.8 mg m<sup>-3</sup> resulted in a no-observable-adverse-effect-level (NOAEL). After extrapolation from rats to humans and from 1 month to 6 months exposure, it was concluded by this group that the PEL should be set around 0.4 mg m<sup>-3</sup>. The toxicology team at Johnson Space Center (JSC) recommended a PEL of 0.5 mg m<sup>-3</sup> in a presentation to the Office of Chief Health and Medical Officer's (OCHMO) staff and to an external committee organized through NASA's Research and Education Support Services in December 2013. The committee generated a report recommending the establishment of the PEL, which was later revised from 0.5 to 0.3 mg m<sup>-3</sup> based on recommendations from the review committee. The final PEL of 0.3 mg m<sup>-3</sup> was presented to the Medical Policy Board in April 2014 and officially accepted by NASA (Scully & Meyers, 2015).

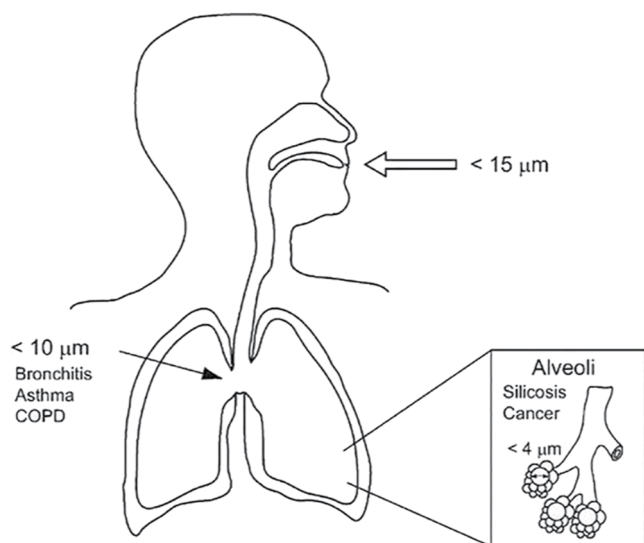


**Figure 1.** Particle settling within the human respiratory system as a function of grain size. Figure from Horwell (2007)—Reproduced by permission of The Royal Society of Chemistry.

## 1.2. A Brief Primer on Lung Interaction With Particulate Matter

Our lungs are a vast network of fluid-filled regions including the alveoli, bronchioles, and interstitial space. About 500 mL of fluid is in the interstitial space with approximately 65 and 36 mL total of fluid stored in the capillaries and alveoli, respectively (Fronius et al., 2012; Lewis et al., 1959; Lindert et al., 2007). The alveoli comprise a majority of the surface area of the human lungs and contain a foam like network that is constituted of a 900:1 ratio of gas: fluid, the fluid being referred to as alveolar fluid (Scarpelli, 2003). The average coating thickness of the alveolar fluid is approximately 0.2 μm (Bastacky et al., 1995). Alveolar fluid plays a critical role in gas exchange and in preventing the alveoli from desiccating (Fronius et al., 2012). The alveolar fluid also functions as a barrier to outside particulates and as an environment for alveolar macrophages (Lambrecht, 2006). Dust particles approximately <4 μm have the ability to settle within the alveoli. This has many health implications regarding astronaut health and safety as a significant portion of the lunar surface contains submicron size dust particles (Park et al., 2008). Inhaled particles will adsorb onto biomolecules such as proteins from surrounding fluids before interacting with cells or alveolar macrophages and some of these proteins may be destroyed by oxidation via OH\* generated from the inhaled particles (Turci et al., 2010). The particles are then detected as foreign objects which are then subsequently absorbed by macrophages.

The macrophages will either mechanically remove the particle from the respiratory system, or it will be unsuccessful in doing so. In the latter case, the particle will go continuously through this cycle which causes chronic inflammation and various respiratory diseases (Linnarsson et al., 2012). As a result, these particles are in constant contact with biological fluids which can then generate ROS and lead to cell apoptosis. Olivine and lunar dust can generate very large quantities of ROS in solution which may then lead to oxidative stress that in turn can damage both epithelial and endothelial cells (Hendrix et al., 2019; Wallace et al., 2009, 2010; Xu et al., 2020). Damaged macrophages due to ROS generation may impede macrophage clearance which would then mean that lunar dust particles may reside in the lungs for extended periods of time (Bos et al., 2019). Studies involving a 3D “lung on a chip” model that replicated the alveolar-blood barrier demonstrated the ability of ROS-generating material to effectively penetrate the alveolar-blood barrier (Xu et al., 2020). Since lunar dust has a high ability to generate ROS, it also has the potential to introduce many lunar dust grains containing olivine to penetrate this membrane as well. Lunar agglutinates contain many pores due to the space weathering process, which in turn causes an increase in their surface areas (Heiken et al., 1991). Since particle clearance is slower for high surface area materials, it is very likely that inhaled lunar agglutinates containing olivine will be cleared from the body at much slower rates than terrestrial particulate matter (Bos et al., 2019). As a result, lunar particulates can remain trapped in the human lungs indefinitely and the long-term effects, including metal release are poorly understood. While studies have shown particles approximately 2–3 μm in diameter are the most efficiently phagocytosed, particles that deviate from that range are not as efficiently engulfed by macrophages (Champion et al., 2008). This implies that lunar dust <2 μm and 3–10 μm in diameter would settle in the human respiratory tracts and potentially remain bioaccessible for extended periods of time (Figure 1). Larger particles may be phagocytosed but fail and repeat via a process known as “frustrated phagocytosis” which may result in more oxidative damage to lung tissues. The long-term consequences of this are not understood and this work attempts to better understand how inhaled lunar dust particles behave over time.

It should be noted that many of these previously mentioned studies extrapolate the toxicity results of rats to humans which may not translate to actual human toxicity due to rats being much more sensitive to biological stimuli than humans (Bos et al., 2019; Driscoll & Borm, 2020). The differences between rats and humans make it difficult to draw definitive conclusions regarding the toxicity of poorly soluble particulate matter (Driscoll & Borm, 2020). Whether poorly soluble particles (PSP) should be considered carcinogenic or not, is dependent on both epidemiological data and studies involving other animals such as mice, hamsters, primates, etc (Driscoll & Borm, 2020). For example, studies working with diesel and coal particulates



show a significant portion of those particles trapped in the alveoli of rats but more or less evenly distributed between the alveoli and interstitium, which is the space between the alveolar epithelium and capillary endothelium, in monkeys (Nikula et al., 1997). In another study involving coal dust in humans, it was reported that approximately 70% of coal dust was in the interstitium and 30% was in the alveolar regions (Nikula et al., 2001). Particles in humans are cleared through more complex mechanisms than rats which include clearance via the mucociliary escalator, alveolar macrophage clearance, and translocation into the interstitium with drainage into the lymph nodes (Bos et al., 2019).

This risk to astronauts is illustrated by well-documented health effects of inhalation exposure to dust released in manufacturing processes and through environmental release (Middleton, 1936). The alveolar macrophages play a critical role through phagocytosis—essentially encapsulation, isolation, and purging of particles. Through this process, alveoli maintain a sterile environment (Ng et al., 2004). However, there is limit to the efficacy of macrophages in their ability to clear particles and some particles are more challenging than others due to their shape (e.g., asbestos fibers), chemical resistance (e.g., quartz), or chemical reactivity (i.e., iron-containing particles). Any of these three factors along with the number of particles entering the lung will determine whether the macrophages can maintain a sterile environment in the alveoli. If phagocytosis is not capable of purging the particles it will compromise the alveolar fluid layer. Alveolar fluid balance is important in maintaining the large amount of water that is exhaled per day from the lungs, approximately 700 mL/day (Fronius et al., 2012). One major way to maintain this fluid balance is through ion transport. Inhaled lunar dust has the potential to release ions such as  $\text{Fe}^{2+}$ ,  $\text{Mg}^{2+}$ , etc. which can possibly interfere with ion transport in the alveoli. Damage and/or oxidation to cells and proteins that regulate fluid transport in and out of the alveolus can lead to alveolar edema or fluid buildup in the alveoli (Zhu et al., 2001). As previously mentioned, many geological samples have been shown to be highly reactive, which means that regulatory cells have the ability to be oxidized by mineral dusts. Buildup of lunar dust in astronaut lungs through time has the potential to lead to alveolar edema. It is therefore very important to further investigate how mineral particles dissolve in lung fluid to better understand how lunar dust inhalation may interfere with alveolar processes. Mortality rates of patients with pulmonary diseases can be as high as 60% with those with below maximum alveolar fluid clearance capabilities and around 20% with maximum alveolar fluid clearance (Sloniewsky et al., 2004). Inhaled olivine particles can be chemically attacked by alveolar macrophages or naturally removed by a variety of methods from the respiratory system, the primary mechanisms being via alveolar macrophages and via the mucociliary escalator (Linnarsson et al., 2012; Oberdorster et al., 2005; Schoonen et al., 2006). Inhaled olivine and lunar dust can settle in different parts of the respiratory system as a function of grain size. Figure 1 shows a simplified diagram of the human respiratory system indicating in which regions particles settle as a function of their sizes (Horwell, 2007).

This is concerning as lunar dust is considered the  $<20\ \mu\text{m}$  portion of lunar regolith. Particle size distributions (PSD) of lunar dust have shown sizes down between 10 and 100's nm in diameter which means that any inhaled lunar dust would be able to settle deep in the respiratory system and be potentially absorbed into the circulatory and nervous systems (Oberdorster et al., 2005). Metal release in lung fluid and the precipitation of secondary minerals due to olivine deposition is not well understood. The goal of this work is to understand olivine dissolution in the human lung and the potential implications on lung processes.

### 1.3. Simulating Particle Dissolution in the Lung

In this report, we attempt to assess the particle residence time of lunar dust grains in the human respiratory system. We selected the mineral olivine for our experiments because it has a high capacity for generating ROS in solution, including  $\text{H}_2\text{O}_2$  (Hurowitz et al., 2007; Kaur et al., 2016) and  $\text{OH}^*$  (Cohn et al., 2006; Hendrix et al., 2019; Horwell, 2007; Horwell et al., 2007; Kaur et al., 2016; Wallace et al., 2009, 2010), both of which are thought to be linked to inflammation and long-term deleterious health effects in the human body (Fubini & Hubbard, 2003; Schoonen et al., 2006; Vallyathan et al., 1992, 1997). Inhalation of lunar dust and the olivine contained in it may lead to similar side effects as those observed in silicosis patients and induce inflammatory responses (Caston et al., 2018; Harrington et al., 2012, 2013; King et al., 1945; Porter et al., 2002; Scheuchenzuber et al., 1985). In addition, olivine is an abundant component of the lunar regolith (Heiken et al., 1991), present at  $\sim 1\text{--}10\ \text{wt}\%$  abundance in the  $10\text{--}20\ \mu\text{m}$  fraction of the regolith and

**Table 1**  
*Components and Concentrations of Simulated Lung Fluid*

Component	Concentration ( $\mu\text{M}$ )
$\text{Na}^+$	150.7
$\text{Ca}^{2+}$	0.197
$\text{NH}_4^+$	10.0
$\text{H}_2\text{CHN}_2\text{CO}_2\text{H}$ (glycine)	5.99
$\text{Cl}^-$	126.4
$\text{SO}_4^{2-}$	0.5
$\text{HCO}_3^-$	27.0
$\text{HPO}_4^{2-}$ , $\text{H}_2\text{PO}_4^-$	1.20
$[\text{HOC}(\text{CH}_2\text{CO}_2)_2\text{CO}_2]^{3-}$ (citrate)	0.20
pH	$7.40 \pm 0.10$

particles of such size can settle in the upper respiratory tracts of the lungs (Horwell, 2007; Jurinski & Rimstidt, 2001; Labotka et al., 1980). In some cases, a decrease in mafic components, including olivine, is observed as lunar dust grain sizes decrease (Heiken et al., 1991; Papike et al., 1982). The observed trend for Apollo 16 (lunar highland regolith) samples exhibits the opposite trend, where there is an observed increase in interstitial mafic components (i.e., olivine) as grain size decreases (Papike et al., 1982). Generally speaking, olivine dust exposure-risk is substantially higher on the Moon compared to Earth due to the large abundance of olivine present in respirable form (Gamble, 1986; Heiken et al., 1991). The lunar surface is a very dusty environment compared to Earth and it is very likely that humans will be exposed to a variety of silicate minerals as dusts may not be common (i.e., olivine and feldspar) on Earth, they can still potentially induce inflammatory responses and uncertain long-term effects when exposed to them in an environment such as on the Moon (Porter et al., 2002; Scheuchenzuber et al., 1985). Finally, based on dissolution rate studies conducted in inorganic liquid media (White

& Brantley, 1995), olivine is known to be among the fastest-dissolving silicate minerals, and so our work on dissolution of this phase in biologically relevant media should place a lower limit on mineral particulate lifetimes in the human body. Little is known about how olivine interacts in the human lung, how long it resides, and what secondary mineral phases are precipitated due to olivine dissolution in biologically relevant aqueous media. Here we present new research aimed at understanding the long-term biopersistence of respirable sized olivine particles in SLF, the capability of olivine to continue producing  $\text{OH}^*$  during long term exposure in SLF, and the ways in which olivine particles might alter lung fluid chemistry in the long term.

For our experiments, we have chosen to work with two fluid media to better understand the lifetime of olivine particles in the human body. The first is “SLF,” also known as “Gamble’s solution.” Gamble’s solution was first developed in 1942 in an attempt to replicate the inorganic salts in fluids released by Type II alveolar cells, which are fluids that help facilitate the exchange of  $\text{O}_2$  and  $\text{CO}_2$  between alveoli and the capillaries (Drysdale & Jamieson, 2008; Knudsen & Ochs, 2018). Gamble’s solution has been further modified in some studies by adding amino acids and other organics present in lung fluids (Bauer et al., 1997). This work uses Gamble’s solution modified by the addition of glycine, sulfuric acid, and ammonium chloride, the composition of which is listed in Table 1.

Numerous studies have been conducted using SLF in the past such as the solubility of uranium compounds in the lung environment (Cooke & Holt, 1974). Many studies involving the assessment of potential human health impacts of industrial materials, air pollution, and other man-made materials have been performed through the years. Air pollution is another field of study where SLF is commonly used. Studies involving the assessment of interactions between SLF, particles  $<10 \mu\text{m}$  diameter ( $\text{PM}_{10}$ ), particles  $<2.5 \mu\text{m}$  diameter ( $\text{PM}_{2.5}$ ), and particles  $<1.0 \mu\text{m}$  diameter ( $\text{PM}_{1.0}$ ) have found that toxic metals such as Cu, As, V, and Sb are largely bioaccessible in the human lungs (Wiseman & Zereini, 2014). Recent work in the geological field involving use of SLF has been conducted in determining the bioaccessibility of trace Ni present in soils. Multiple soil samples were collected in and around the mining town of Kalgoorlie, WA, Australia which is also home to a Ni smelting plant. These studies found that the bioaccessibility of Ni increased through time and that greater Ni concentrations are observed in the  $<10 \mu\text{m}$  particles (Drysdale et al., 2012). This is relevant to lunar exploration because it has been shown that trace elements are enriched in the  $<10 \mu\text{m}$  lunar grain size fractions which include Ni, Eu, Sm, Th, Ce, and Dy, as well as others (Papike et al., 1982). Agglutinates, which are a product of space weathering and unique to the lunar surface, contain metallic nanometer sized iron spherules which have unknown toxic properties. Many toxic trace elements present in lunar soils would be highly bioaccessible once in the human lungs, which has numerous human health implications. Our olivine samples contain approximately  $400 \text{ mg kg}^{-1}$  Ni and the results from Drysdale et al. (2012) show that one sample in that study with approximately the same Ni concentration, demonstrated the highest bioaccessibility compared to other samples tested. Results from Drysdale et al. (2012) demonstrated that addition of amino acids to SLF can significantly increase bioaccessibility of toxic metals such

as Ni. A study using volcanic ash determined that different elements exhibited different leaching behaviors depending on the SLF composition and other testing parameters (Tomašek et al., 2021). It was found that Fe release varied the most and that Mg release varied the least upon modification of the SLFs used, including deionized water. The main elements in olivine are Fe, Mg, and Si so unless Mg release is the only element being measured, then it is appropriate to use a biological fluid to understand the bioaccessibility of olivine. The SLF used in this work does not contain complex proteins (which are made up of amino acids) found in lung fluids, which may result in underestimation of the bioaccessibility of toxic trace metals of air pollution, natural soils, and other man-made materials (Harrington et al., 2012).

The other fluid used in our experiments is 0.1 M HCl. For our experiments, we used a 0.1 M HCl solution prepared by diluting stock (12 M) HCl with ultrahigh purity (18 M $\Omega$ ) water to a pH of  $1.3 \pm 0.1$ . Hydrochloric acid is a medium that is frequently used in mineral dissolution rate studies, and there is a significant body of literature on olivine dissolution in acid media such as HCl (Crundwell, 2014; Luce et al., 1972; Oelkers et al., 2018; Pokrovsky & Schott, 2000; Rosso & Rimstidt, 2000; Wogelius & Walther, 1991), which provides us with the ability to compare our dissolution rate measurements in HCl against published estimates in order to ensure that our experimental methods (described below) yield rates that are in good agreement with previous estimates. Conveniently, gastric acid also consists largely of HCl and other dissolved constituents. Simulated Gastric Fluid (SGF) of the fasted stomach is typically prepared as a mixture of HCl (0.2M) and NaCl (0.3 M) dissolved in water (with or without pepsin, which is a digestive enzyme), with a final pH of 1.2 (Klein, 2010). While our HCl lacks the dissolved NaCl typical of SGF, olivine dissolution rates are understood to be largely unaffected by the salinity of a solution (Oelkers et al., 2018). Thus, the dissolution rates we measure in HCl might be considered a reasonable first approximation for addressing the lifetime of inadvertently ingested regolith mineral constituents. A fully thorough analysis of ingested lunar analog material would entail the implementation of the bioaccessibility test developed by the BioAccessability Research Group of Europe (BARGE) known as the Unified BARGE Method (UBM). This procedure involves testing the bioaccessibility of particles in simulated digestive fluids which include saliva, gastric fluid, duodenal fluid, and bile. Studies have shown that there is a correlation between dust exposure and cancers of the colon and stomach (García-Pérez et al., 2015; Santibañez et al., 2012). These studies indicate that there is a pressing need to explore the potential hazards of lunar dust ingestion in future work.

This work uses both measured dissolution rate calculations and geochemical modeling to understand the fate of particulate lunar material in the human respiratory system years after initial exposure. Current studies and data pertaining to lunar dust toxicology only assess short-term impacts of lunar dust exposure on human health. Short-term impacts of lunar dust inhalation can induce oxidative damage to lung and other tissues, but long-term impacts may be caused by lunar dust dissolution and reprecipitation into other mineral phases. This work is the first to our knowledge to advance understanding of the potential hazard posed by lunar dust exposure on human health by dissolving olivine, a common mineral found in lunar dust, and assess both the oxidative potential and secondary mineral precipitation over time.

## 2. Materials and Methods

### 2.1. Materials

Olivine having the composition Fo<sub>91</sub> was obtained from a mineral collection curated by M. D. Dyar at Mount Holyoke College. The composition of the olivine was determined by X-Ray Fluorescence (XRF) and X-Ray Diffraction (XRD) (Byrne et al., 2015; Hendrix et al., 2019). The olivine sample was crushed in a steel mortar and pestle before being sieved using a 63  $\mu$ m sieve. The <63  $\mu$ m fraction was then removed and further crushed in a Retsch PM 100 agate ball mill grinder at 350 rpm for 2 hr. Agate ensured minimal contamination for processing olivine samples (Hickson & Juras, 1986).

### 2.2. SLF and HCl Preparation

500 mL of SLF was prepared using the methods outlined in Bauer et al. (1997). The concentration of each component of SLF can be found in Table 1. A solution of 0.1 M HCl was prepared using reagent-grade HCl (12 M) and ultra-high purity (18 M $\Omega$ ) water. Experiments were conducted with the HCl solution as a control to understand whether our flow-through apparatus could be used to reliably reproduce published mineral

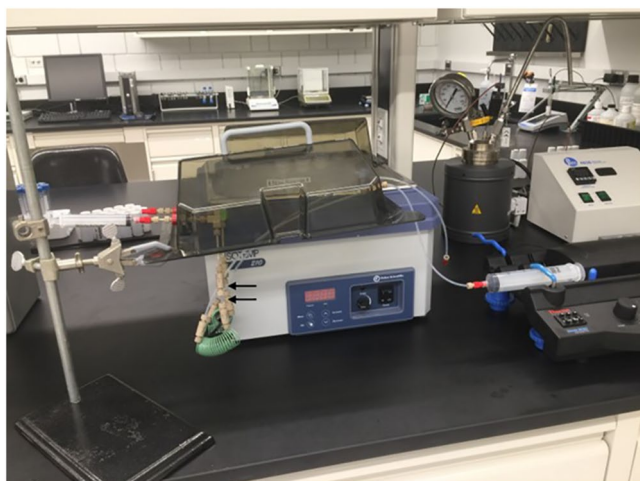


**Figure 2.** Set up of the flow-through experiments with the tubing unsubmerged in the water bath for clarity. A 60 mL syringe tube (right) is filled with either simulated lung fluid or 0.1 M HCl which is pumped at a rate of 0.13 mL/hr. The solvent moves through the tubing, then the sample chambers (denoted by black arrows) before effluent is collected in a 10 mL syringe on the opposite end of the set up.

dissolution rates for olivine dissolved in acid media under similar temperature conditions, while also providing dissolution rate information relevant to olivine particle survival in gastric fluid.

### 2.3. Flow-Through Apparatus

Dissolution experiments were conducted in a packed-bed flow-through reactor apparatus modeled after the one described in Gainey et al. (2014) and Hurowitz et al. (2005). The apparatus, shown in Figure 2, consists of a Fisher Scientific Isotemp 210 water bath, a Thermo Scientific Orion M362 dual-channel syringe pump, PEEK and PFA tubing (including the unions and ferrules needed to make connections between lengths of tubing), and inline PEEK filter frit discs (2 μm pore size) used to ensure that the solid sample stays in the packed-bed sample chamber during experimentation. Two sets (A and B) of flow-through tubing and sample chambers were constructed to make identical flow-through lines, which were connected to the syringe pump.

All tubing was then acid washed prior to experimentation by pumping 10% HCl through the tubing using the syringe pump, then DI water, then finally pumping air through the line to dry the tubing out. Between 65 and 85 mg of olivine sample was then loaded into each sample chamber, and the sample chambers including the tubing were then submerged in the water bath, which was kept at 37°C in order to replicate internal human body temperature.

The sample chambers were placed at the end of 260–270 cm of submerged tubing (including a 200 cm length of coiled tubing placed immediately before the sample chamber). Two 60 mL syringes were loaded onto the syringe pump, each filled with approximately 50–55 mL of fluid. The fluid was injected into the flow-through reactor by the syringe pump at a flow rate of 0.13 mL hr<sup>-1</sup> for both channels, which depleted the fluid in the syringe over an approximately two-week period. Given the known tubing lengths, diameters, and fluid flow rate, we calculate that the solvent flowed for a minimum of 1.5 hr in the submerged tubing before reaching the sample, thus ensuring that the fluid was warmed up to 37°C before coming into contact with the olivine inside the submerged sample chamber. Effluent was collected after it had passed through the packed-bed reactor using 10 mL syringes that were connected to the outlet end of the reactor system. Samples were collected at intervals ranging from 24 to 72 hr after experiment start. Effluent volumes varied at times, hence the 24–72-hr time frame between sample collections. Table 2 shows the total experiment time, olivine mass loaded, and number of solution samples collected for each sample run.

### 2.4. pH Measurements

The pH of each effluent sample was measured using a Fisher Scientific Accumet Basic AB15 pH meter. The instrument was calibrated with Orion Application Solutions pH 4, 7, and 10 standards.

### 2.5. ICP-AES Analysis

A Thermo iCAP 6300 radial view Inductively Coupled Plasma-Atomic Emission Spectrometer (ICP-AES) was used to analyze Fe, Mg, and Si concentrations. Prior to analysis, 1 mL of each sample was pipetted into a sterile 15 mL centrifuge tube, and 6 mL of 10% HCl was then added to the sample. Standards with concentrations of 0.1, 1.0, and 10.0 ppm Fe, Mg, and Si were prepared from 10,000 ppm certified ICP spectral standards (Alfa Aesar) using the same 10% HCl as a dilutant. Limits of detection (LOD) for Fe, Mg, and Si were determined to be 6.0 ppb (1.07 × 10<sup>-7</sup> M), 0.6 ppb (2.47 × 10<sup>-8</sup> M), and 48.4 ppb (1.72 × 10<sup>-6</sup> M), respectively.

**Table 2**  
Total Experiment Time, Olivine Mass Loaded, and Number of Solution Samples Collected for Each Sample Run

0.1 M HCl Run #	Total time (h)	Olivine mass (mg)	Number of samples	SLF Run #	Total time (h)	Olivine mass (mg)	Number of samples
1	280	48.6	15	1	360	83.8	22
2	348	83.8	20	2	360	78.3	22
3	356	66.5	11	3	375	77.8	12
4	356	67.7	11	4	375	77.5	12
5	407	91.9	10	5	406	46.1	7
				6	406	50.1	7

Note. All runs conducted at 37°C and a flow rate of 0.13 mL/hr.



**Table 3**  
Concentration Values Entered Into PHREEQC v3.5

Species	0.1 M HCl (millimolar)	SLF (micromolar)
Fe	4.0	6.1
Mg	38	81
Si	18	43
Cl	100	126
O <sub>2</sub>	0.2	200
CO <sub>3</sub> <sup>2-</sup>		27
Ca		0.197
NH <sup>4+</sup>		10
Na		150.7
P		1.2
SO <sub>4</sub> <sup>2-</sup>		0.5

## 2.6. Solid Phase Characterization

Average grain sizes were determined on unreacted olivine using a Malvern Instruments Mastersizer 2000, which measures particle sizes by measuring the intensity of scattered light by particles suspended in deionized water in triplicate. Surface areas of samples were measured using ultra high purity nitrogen via six-point Brunauer, Emmett, and Teller (BET) theory on a NOVA-2000 BET analyzer. Approximately 250 mg of olivine reacted in SLF and 10 mg of olivine reacted in 0.1 M HCl were analyzed using six-point BET. A LEO-1550 FEG scanning electron microscope (SEM) equipped with an energy dispersive X-ray (EDAX) spectrometer was used to obtain images and information on the elemental composition of olivine one time before reaction and then one time each after reaction in both 0.1 M HCl and SLF. A Rigaku MiniFlex 600 X-ray diffractometer (XRD) was used to assess any changes in mineralogy of the samples before and after dissolution. For XRD analysis of reacted olivine, samples were removed from the sample chambers after dissolution and subsequently ground in an agate mortar and pestle for about 30–60 s with approximately 1–2 mL of acetone. A small amount of slurry was pipetted onto the underside of a zero background XRD sample plate and

allowed to dry before collecting XRD spectra. Attenuated Total Reflectance (ATR) spectra were collected on a Nicolet 6700 Fourier Transform Infrared (FTIR) spectrometer purged of both water and carbon dioxide. The spectrometer was equipped with a SmartOrbit ATR accessory with a 1 mm diameter type IIA diamond ATR element with input and emergence angles of 45°. Spectra were collected at a resolution of 4 cm<sup>-1</sup> at a range of 6,000–350 cm<sup>-1</sup> for a total of 1,024 scans. All spectra were referenced to a background by collecting a spectrum before each sample run using the same settings without adding sample to the diamond element.

## 2.7. OH\* Measurements

In a separate set of experiments, approximately 200 mg aliquots of olivine were hand-ground in an agate mortar and pestle and then mixed with either 0.5 mL of SLF or 0.5 mL 0.1 M HCl for incubation periods of 0, 1, 3, 5, and 7 days. After incubation, 0.5 mL 88.4 mM DMPO, a radical spin-trapping compound was added to the slurry. The samples were incubated for an additional 15 min in order to allow any OH\* present to react with the DMPO. The sample incubated for “0 days” was incubated for only a period of 15 min immediately after grinding. After each incubation period the olivine slurries were filtered using a Millex GN syringe driven 0.20 μm filter and the effluents were pipetted into a 50 μL glass capillary tube. OH\* concentration measurements were then made using a benchtop Magsnetech Electron Paramagnetic Resonance (EPR) X-band spectrometer using techniques described in Hendrix et al. (2019). The EPR parameters used are listed in Supporting Information S1. All OH\* measurements were performed in duplicate.

## 2.8. PHREEQC

PHREEQC is a C/C++-based computer modeling program with a graphical user interface that is designed to perform a variety of aqueous geochemical calculations (Parkhurst & Appelo, 2013). We used PHREEQC v3.5 to determine the mineral saturation state of fluids produced from our experiments. In our PHREEQC simulations, the temperature was set to the water bath temperature of 37°C and the pH was set as the input pH values of 1 and 7.4 for 0.1 M HCl and SLF, respectively. Oxygen values were set at 0.0002 mol kg<sup>-1</sup> which is the solubility of oxygen at 37°C. Table 3 shows the species concentrations (mol kg<sup>-1</sup>) input into PHREEQC. Concentrations of Fe, Mg, and Si used are the average steady state concentrations derived from our flow through experiments. In our simulations, we then balanced the charge of the solution by allowing PHREEQC to adjust pH to the appropriate value, resulting in pH values close to those measured in the outlet solutions of our experiments. PHREEQC input files are available in Supporting Information S1.

### 3. Results

#### 3.1. Dissolution of Olivine in 0.1 M HCl and SLF

The measured concentrations of Fe, Mg, and Si are plotted as a function of time on Figure 3 for 5 separate experiments in which olivine was dissolved in 0.1 M HCl.

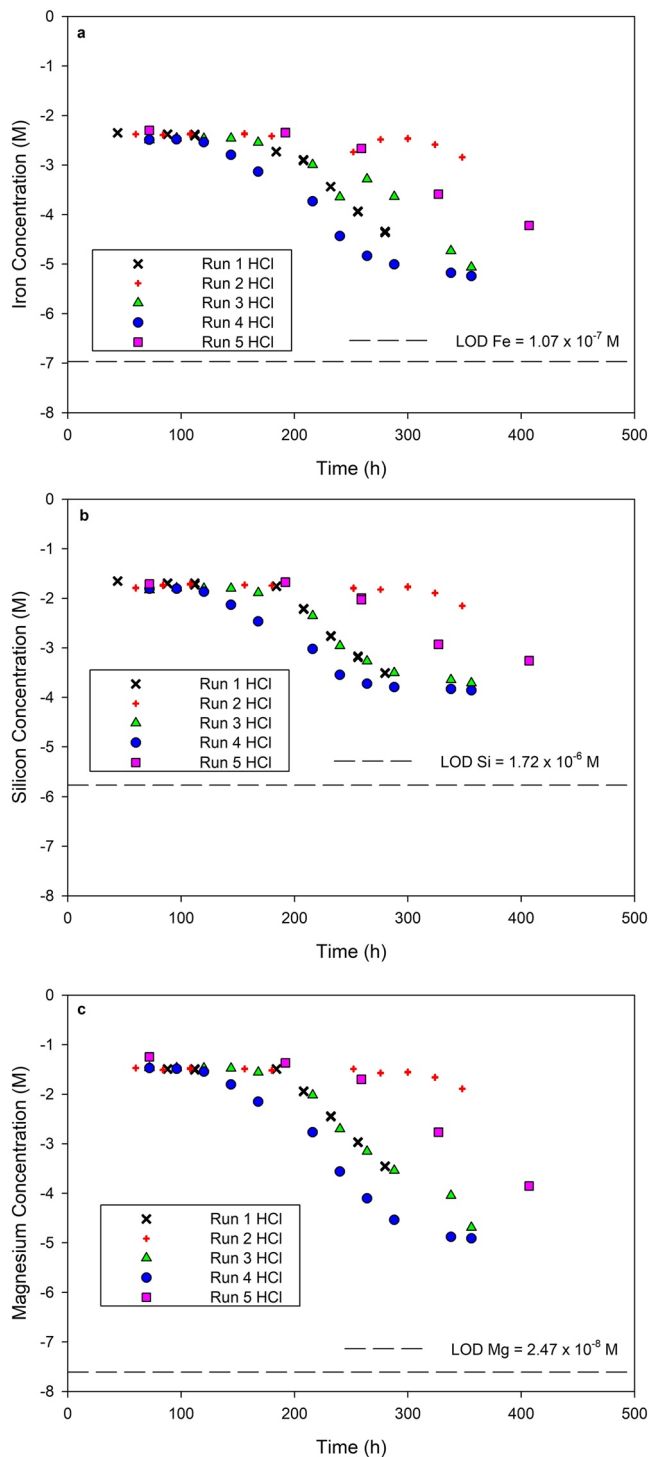


**Figure 3.** Concentration (M) versus time (h) graphs of (a) Fe, (b) Si, and (c) Mg in 0.1 M HCl. LOD, Limit of Detection. Details for each run can be found in Table 2. Note: some data points overlap.

As shown on the graph, the concentrations of these elements generally decrease over the course of the experiment, in the case of Runs 1, 3, and 4, leveling off to their lowest concentrations by ~250 hr. For Runs 2 and 5, the approach to similarly low concentrations appears to take longer, between 300 and 400 hr, which is due to the larger amount of olivine loaded into the sample chamber for these runs (Table 2). On Figure 4a, the molar ratios of Si/Fe, Si/Mg, and Mg/Fe for fluid samples for runs 1, 3, and 4 are plotted as a function of time and compared to the ratios of these elements in the olivine used in our experiments. The same relationships are plotted for runs 2 and 5 on Figure 4b. This allows us to determine if olivine dissolves stoichiometrically or not.

As shown, all solution concentration data prior to 250 hr plot along the ratio defined by the elemental ratios in olivine, indicating stoichiometric dissolution of the mineral. After 250 hr, the data for Runs 1, 3, and 4 depart from the stoichiometric olivine ratios, coincident with the approach to lowest measured solution concentrations in these experiments (Figure 3). For Runs 2 and 5, stoichiometric dissolution is maintained up to approximately 350 hr of dissolution, after which time the fluid ratios depart from those in the solid phase; also coincident with the time period in which we observe the lowest measured solution concentrations.

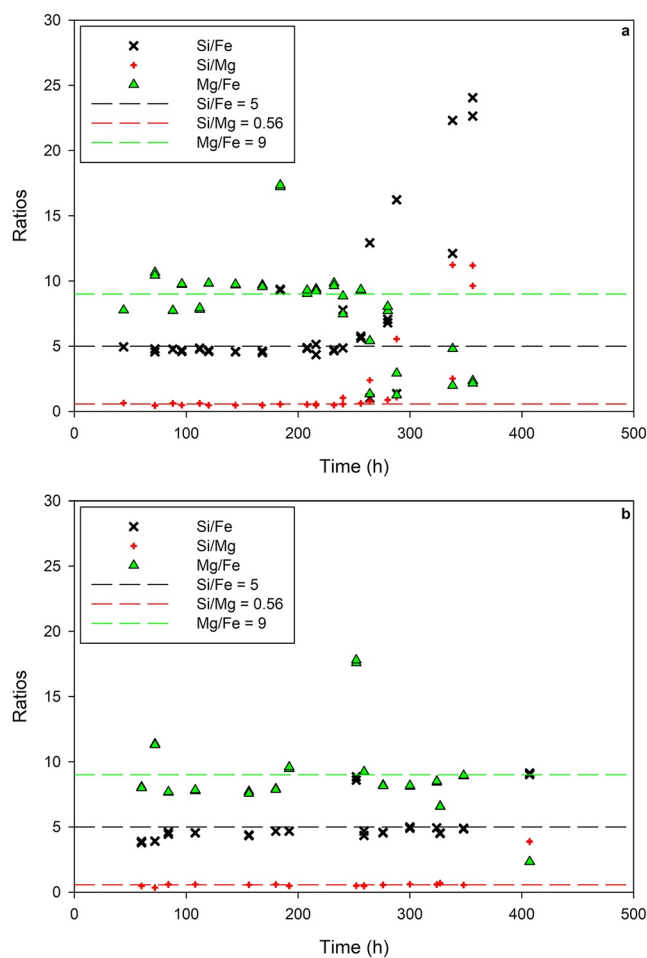


**Figure 4.** Concentration ratios of Si/Fe, Si/Mg, and Mg/Fe in 0.1 M HCl. (a) Runs 1, 3, and 4 (b) Runs 2 and 5. The ratios of the elements present in olivine are denoted by the dashed lines. Note the deviation from stoichiometric dissolution for runs 1, 3, and 4 occurs at approximately 250 hr whereas deviation from stoichiometric dissolution occurs at approximately 350 hr for runs 2 and 5. This is most likely due to the use of greater amounts of olivine for runs 2 and 5 relative to runs 1, 3, and 4 as shown in Table 2. Note: some data points overlap.

Figure 5 shows the measured concentrations of Fe, Mg, and Si over time for olivine dissolution in SLF for 6 separate experiments (we note that only four experiments are plotted on Figure 5a due to iron being below the detection limit in two experiments).

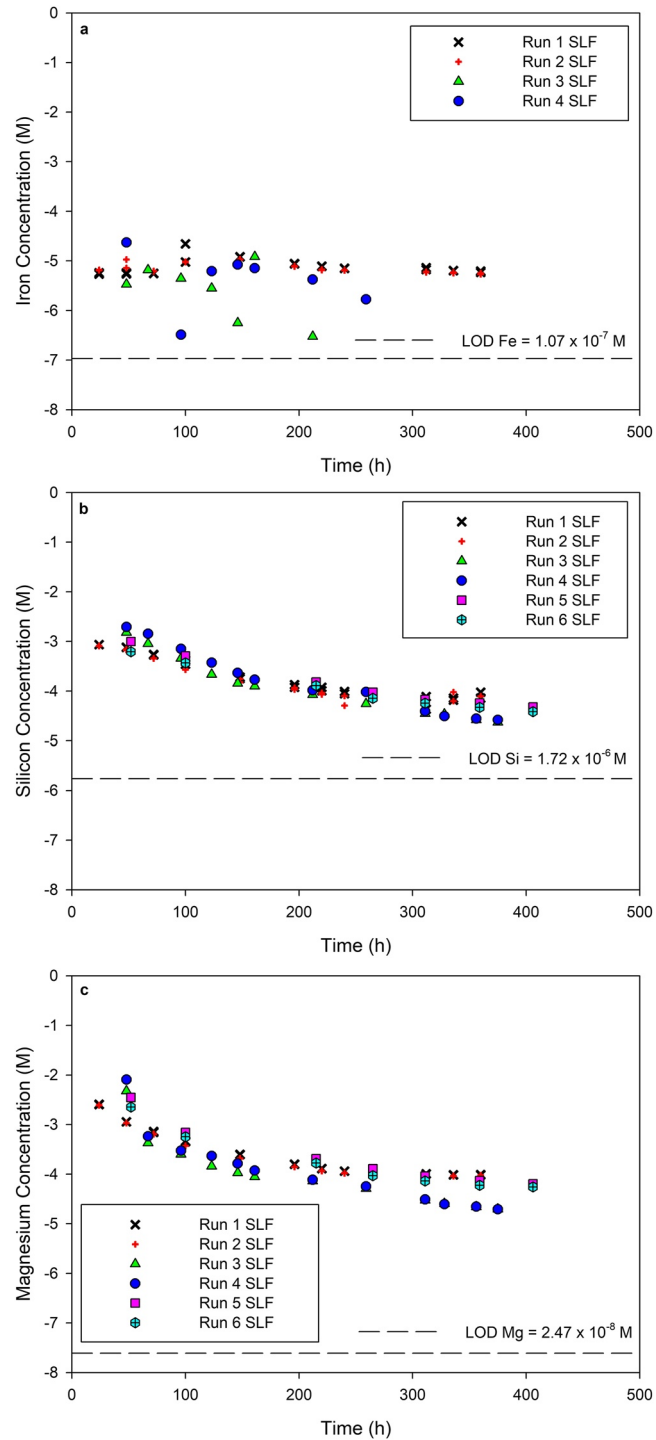


**Figure 5.** Concentration (M) versus time (h) graphs of (a) Fe, (b) Si, and (c) Mg in SLF. LOD, Limit of Detection. Details for each run can be found in Table 2. Fe was below the detection limit for runs 5 and 6. Note: some data points overlap.



As shown, the concentration of Fe scatters around an average value of  $\sim 10 \mu\text{M}$  over the duration of the experimental runs plotted (Note Fe was not detected in samples from Runs 5 and 6). The concentrations of Mg and Si decline over the course of all 6 experiments to  $\sim$ sub millimolar concentrations, leveling off to a steady, low concentration by  $\sim 100\text{--}200$  hr after the start of the experiment (the approach to lowest concentration takes longer for Si than Mg). Overall, the concentration of Fe, Mg, and Si were approximately 2–3 orders of magnitude lower in SLF versus 0.1 M HCl. On Figure 6, the molar ratios of Si/Fe, Si/Mg, and

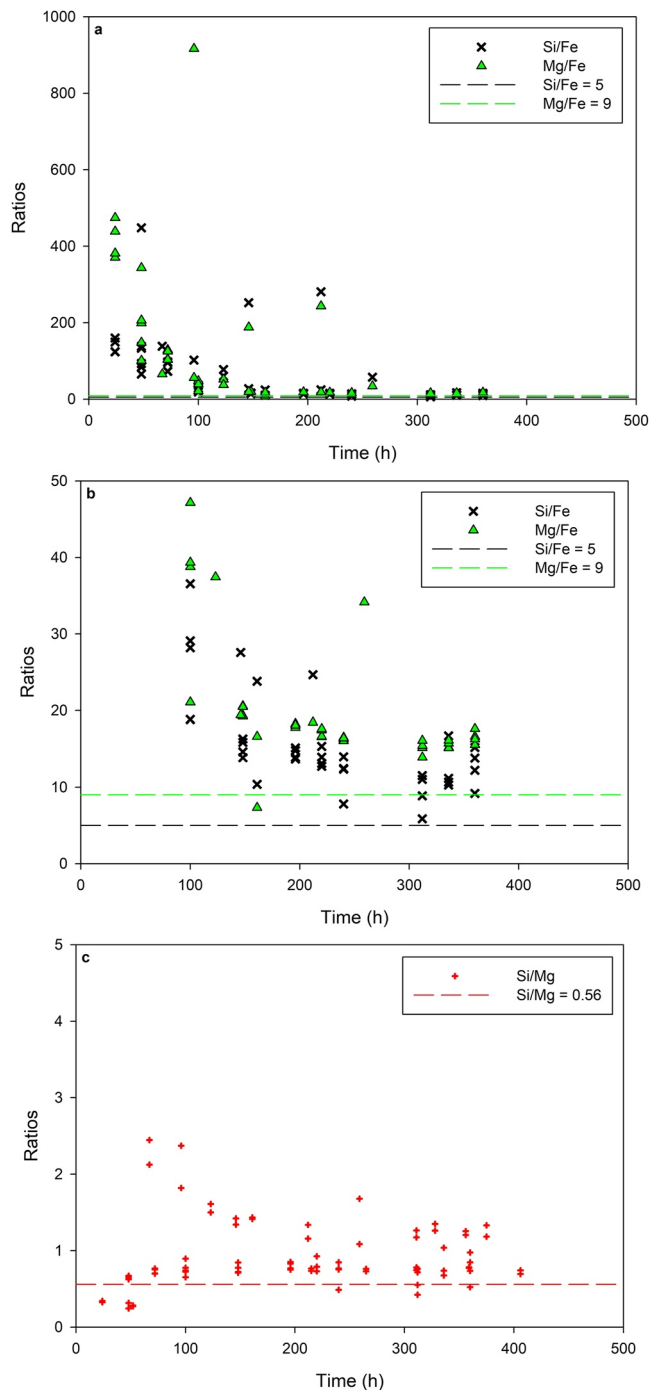


**Figure 6.** Concentration ratios of (a) Si/Fe, Mg/Fe, (b) Si/Fe, Mg/Fe (smaller Y-axis scale) and (c) Si/Mg in SLF; (various Y-axis scales are for clarity). There is no definite stoichiometric dissolution observed for any of the elements released into SLF regardless of initial amount of olivine used during each run. Note: some data points overlap.

Mg/Fe for fluid samples are plotted as a function of time and compared to the ratios of these elements in the olivine for all experiments. As shown on Figures 6a and 6b, the Si/Fe and Mg/Fe ratios are significantly elevated (by factors of 10's to 100's) relative to that of olivine for the early (<200 hr) portion of all experiments and remain elevated by a factor of 2–3 for the latter (>200 hr) portion of the experiments. In contrast, Si/Mg ratios are not as significantly elevated in the early portion of the experiments (Figure 6c), and level off to Si/Mg ratios that are elevated only by a factor of ~2 relative to the Si/Mg ratio in olivine after ~200 hr of dissolution.

### 3.2. pH Measurements

pH measurements were conducted on aliquots recovered from both dissolution in SLF and 0.1 M HCl and are plotted as a function of time on Figure 7.

The initial pH of the 0.1 M HCl stock solution was  $1.3 \pm 0.1$  and the pH of the SLF stock solution was  $7.4 \pm 0.1$ . As shown on Figure 7, for experiments conducted with 0.1 M HCl, pH starts approximately at 3.8–3.9 then slowly declines over time to a value of ~2, closer to that of the inlet fluid. In experiments with SLF, the pH is elevated relative to that of the inlet solution, at pH 8.0–9.0, and remained at this level through the duration of the experiment. A slightly elevated pH value is noted at the start of the experiment relative to subsequent measurements.

### 3.3. SEM Analysis

SEM images reveal clear differences between the effects of dissolving olivine in SLF versus 0.1 M HCl. Olivine grains dissolved in SLF are indistinguishable from fresh, unreacted olivine. Figure 8 shows olivine grains at 50000X magnification that were (a) not exposed to any solvent, (b) dissolved in SLF, and (c) dissolved in HCl.

Comparing Figures 8a and 8b shows no discernable difference between undissolved olivine versus olivine reacted with SLF. Figure 8c show olivine grains that were exposed to 0.1 M HCl. It can be seen in Figure 8c that dissolution in 0.1 M HCl left an amorphous-looking precipitate behind on the mineral surface. EDX spectra were obtained on all samples, which show clear distinctions between olivine dissolved in SLF versus 0.1 M HCl. Figure 9a shows the EDX spectra of unaltered olivine and Figures 9b and 9c shows the EDX spectra of olivine dissolved in both SLF, and 0.1 M HCl, respectively. The EDX spectra of unaltered olivine and olivine dissolved in SLF look identical whereas the EDX spectrum of olivine dissolved in 0.1 M HCl has

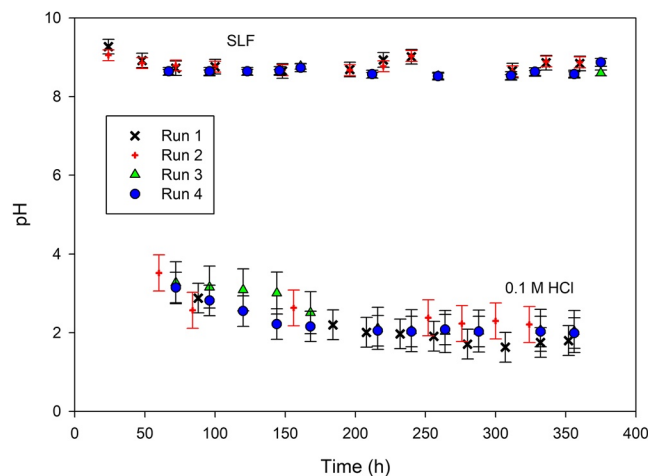


**Figure 7.** pH versus time (h) of olivine dissolution in 0.1 M HCl and SLF. There was not enough effluent collected in order to measure pH values for runs 5–6. Note: the data set between pH 8–10 represents olivine dissolution in SLF and the data set between pH 1–4 represents olivine dissolution in 0.1 M HCl.

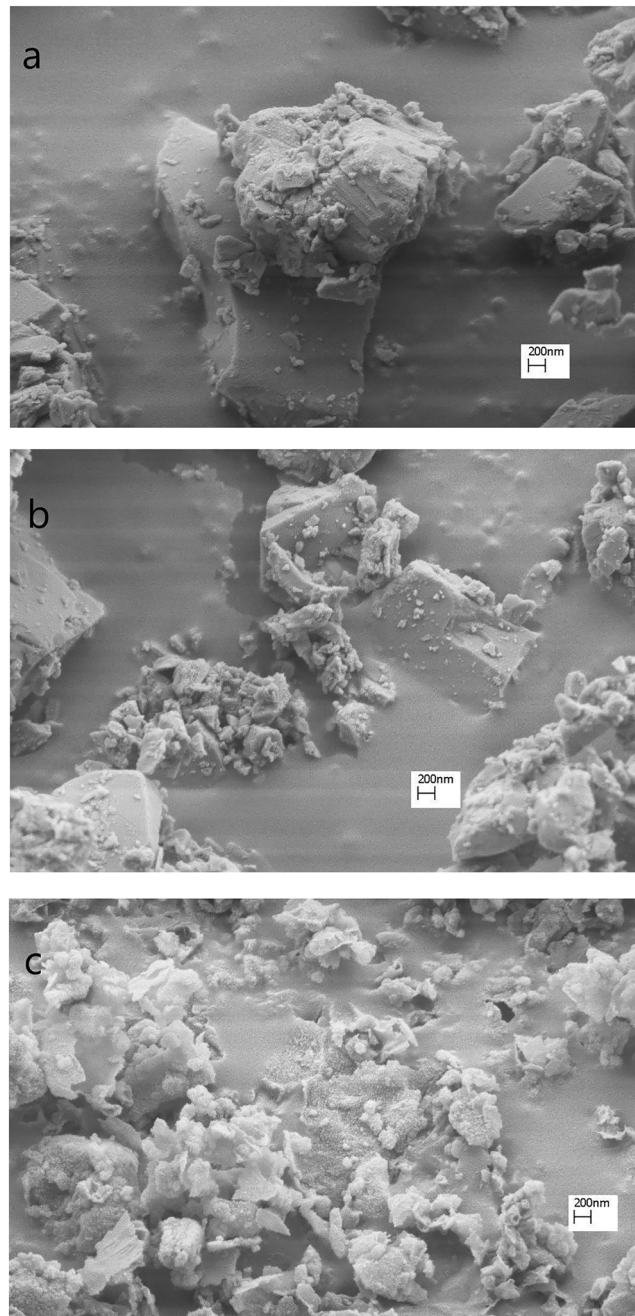


**Figure 8.** SEM images of olivine at a scale of  $0.2 \mu\text{m}$  (50000X magnification) (a) unreacted, (b) dissolved in SLF, and (c) dissolved in 0.1 M HCl.

a relatively large Si peak compared to Fe and Mg, indicating the presence of either a Si-enriched residue and/or Si-rich surface precipitate.

### 3.4. Grain Size and Surface Area Analysis

The median grain size for olivine used in the experiments was approximately  $7.55 \pm 0.72 \mu\text{m}$ , which is well within the respirable range of particulate matter outlined in Figure 1. Specific surface area analysis of 6 separate unaltered olivine samples gives an approximate average value of  $3.0 \pm 0.71 \text{ m}^2 \text{ g}^{-1}$ . Following

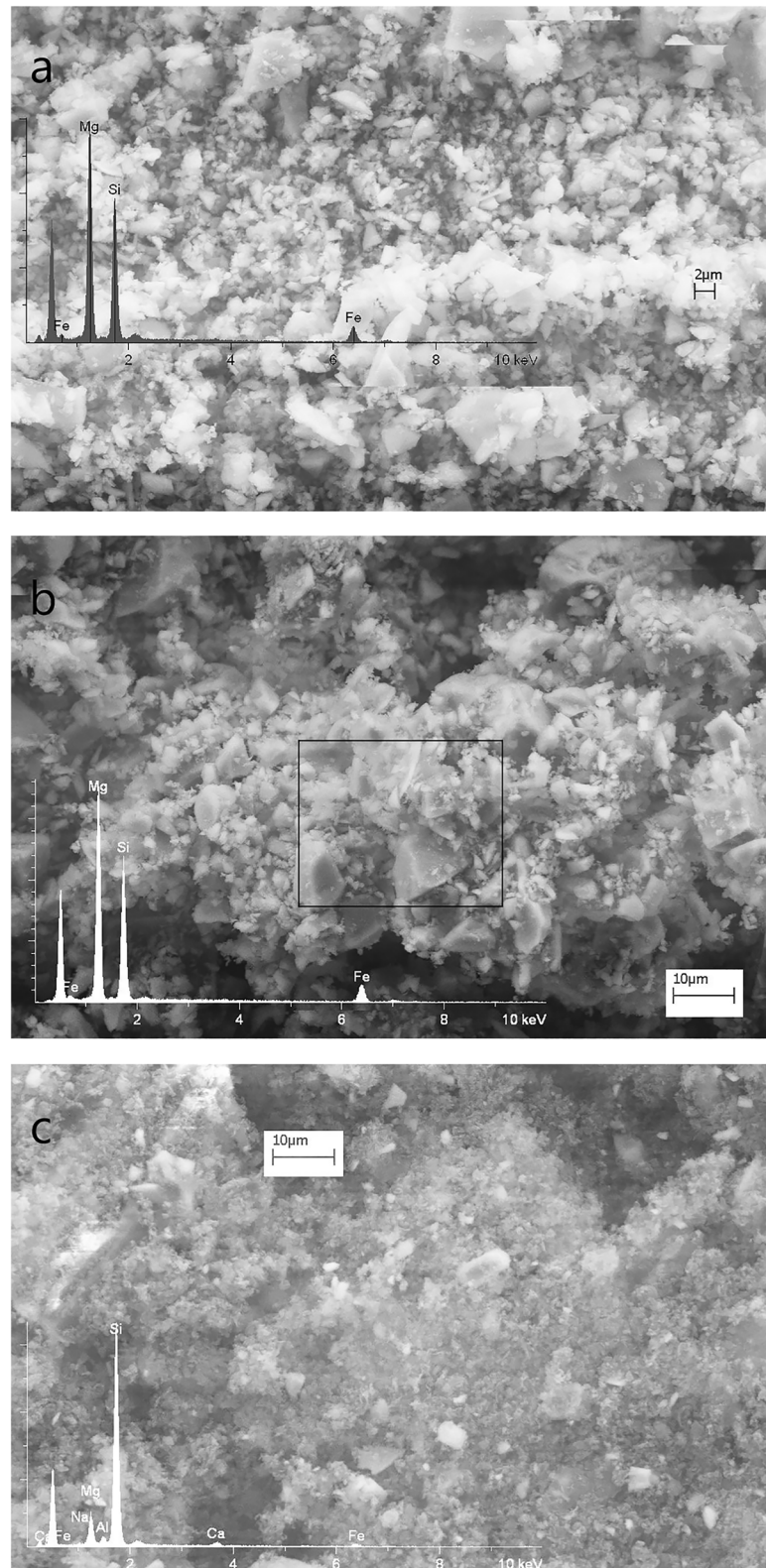


**Figure 9.** EDX spectrum of (a) undissolved olivine, (b) olivine dissolved in SLF, and (c) olivine dissolved in 0.1 M HCl. Note: box in Figure 9b denotes area where EDX spectrum was measured.



dissolution in 0.1 M HCl and SLF, olivine surface areas increased to an average of  $61.6 \text{ m}^2 \text{ g}^{-1}$  and  $4.56 \text{ m}^2 \text{ g}^{-1}$ , respectively. Raw data for olivine grain size and surface areas, including uncertainties can be found in Supporting Information S1.

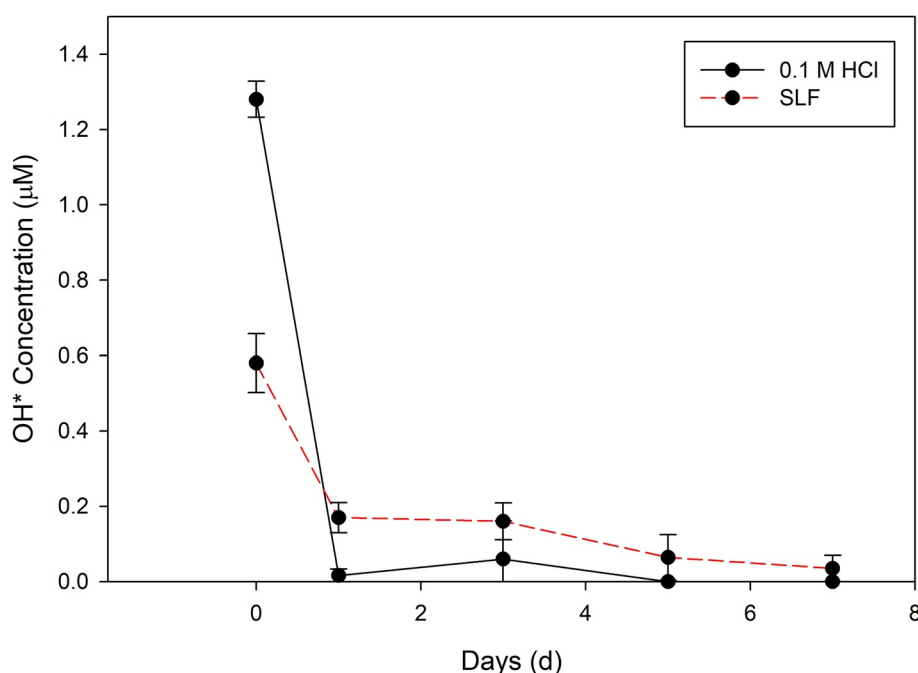
### 3.5. OH\* Measurements

Figure 10 shows the generation of OH\* by olivine powder in both 0.1 M HCl and SLF. Initially the amount of OH\* generated by olivine in 0.1 M HCl is about double that generated by olivine incubated in SLF. After approximately 24 hr the concentration of OH\* generated rapidly subsides in both sets of experiments. The decline in OH\* generation may be slower for olivine incubated in SLF than in HCl, though only the 0- and 24-hr incubations can be reliably distinguished from each other within the measurement uncertainties.

### 3.6. XRD Analysis

The XRD spectra for olivine dissolved in both 0.1 M HCl and SLF are lower in intensity relative to fresh, unaltered olivine. This is because relatively small amounts of sample were recovered from the dissolution experiments, making for a dilute slurry during XRD sample preparation. Despite this, Figure 11a shows a dramatic change in the XRD pattern of olivine dissolved in 0.1 M HCl: only two peaks clearly rise above the background scatter in the XRD pattern, at  $\sim 28^\circ$  and  $31^\circ 2\theta$ , in positions similar to peaks that are present in the unaltered olivine XRD pattern. This observation is due to the olivine crystal structure being “lost” during dissolution in HCl. The two matching peaks between reacted and unreacted olivine are likely some remnant olivine left over in its crystal form even after dissolution in 0.1 M HCl.

There is also a broad “hump” in the XRD pattern for olivine dissolved in 0.1 M HCl, centered around  $26^\circ 2\theta$ , consistent with the presence of an amorphous phase, likely the Si-rich material detected by SEM/EDX. In contrast, the XRD pattern for olivine dissolved in SLF (Figure 11b) is similar to that of unaltered olivine, containing the expected XRD peaks for olivine, though lower in overall intensity due to the aforementioned sample XRD preparation method. There is only one component of the spectrum for olivine dissolved in SLF that is not readily explained as originating from olivine, and that is a broad peak centered at  $\sim 13\text{--}14^\circ 2\theta$ .



**Figure 10.** Plot of OH\* concentration ( $\mu\text{M}$ ) versus time (d) for samples incubated in SLF and 0.1 M HCl. Error bars indicate the standard deviation for duplicate runs.

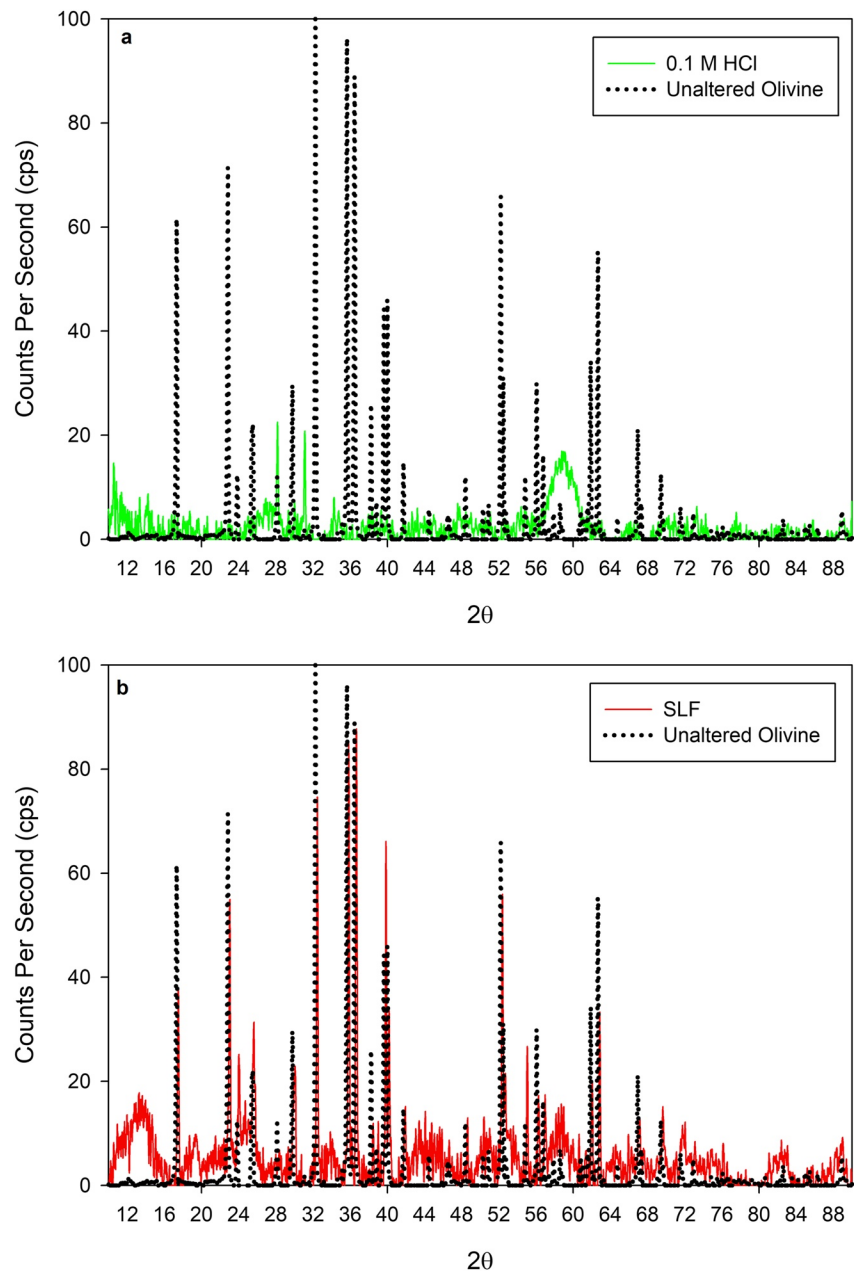


**Figure 11.** (a) XRD spectra of unaltered olivine and olivine dissolved in 0.1 M HCl. (b) XRD spectra of unaltered olivine and olivine dissolved in SLF.

A number of Mg-phyllsilicate minerals (e.g., chrysotile, clinochlore, and chamosite) exhibit intense basal XRD reflections at around this  $2\theta$  angle, and so it is possible that this broad peak indicates the presence of a poorly crystalline Mg-phyllsilicate precipitate formed during the experiment. Finally, there is an additional broad peak centered at  $59^\circ 2\theta$  in the XRD patterns for olivine dissolved in 0.1 M HCl and SLF that originates from the sample holder.

### 3.7. ATR-FTIR Analysis

Figure 12 shows the ATR-FTIR spectra of olivine dissolved in both SLF and 0.1 M HCl compared to spectra of unaltered olivine, hydrated silica, quartz, and ferrihydrite. Notable features in the spectra include broad

peaks at  $1,637\text{ cm}^{-1}$  and  $3,286\text{ cm}^{-1}$  in the spectra of olivine dissolved in 0.1 M HCl, which match well to similar peaks in the spectrum of ferrihydrite. In ferrihydrite, such features are attributed to water in the mineral structure. There is a peak at  $1,071\text{ cm}^{-1}$  in the spectrum of olivine dissolved in 0.1 M HCl, and a shoulder at  $1,200\text{ cm}^{-1}$ , that align with similar features in the spectra of quartz and silica. XRD results from the olivine dissolved in 0.1M HCl are inconsistent with the presence of quartz and indicate that these features are more likely due to amorphous silica. Hydrated amorphous silica has a doublet at  $1,637\text{ cm}^{-1}$  and a triplet in the  $2,700\text{--}3,800\text{ cm}^{-1}$  region. The olivine dissolved in 0.1M HCl also has broad peaks in both of these locations that may be due to amorphous silica, however, as described above, these features appear to be more closely associated with spectral absorptions characteristic of ferrihydrite. As can also be seen in Figure 12, there is no observable difference in the spectra of olivine dissolved in SLF and unaltered olivine.

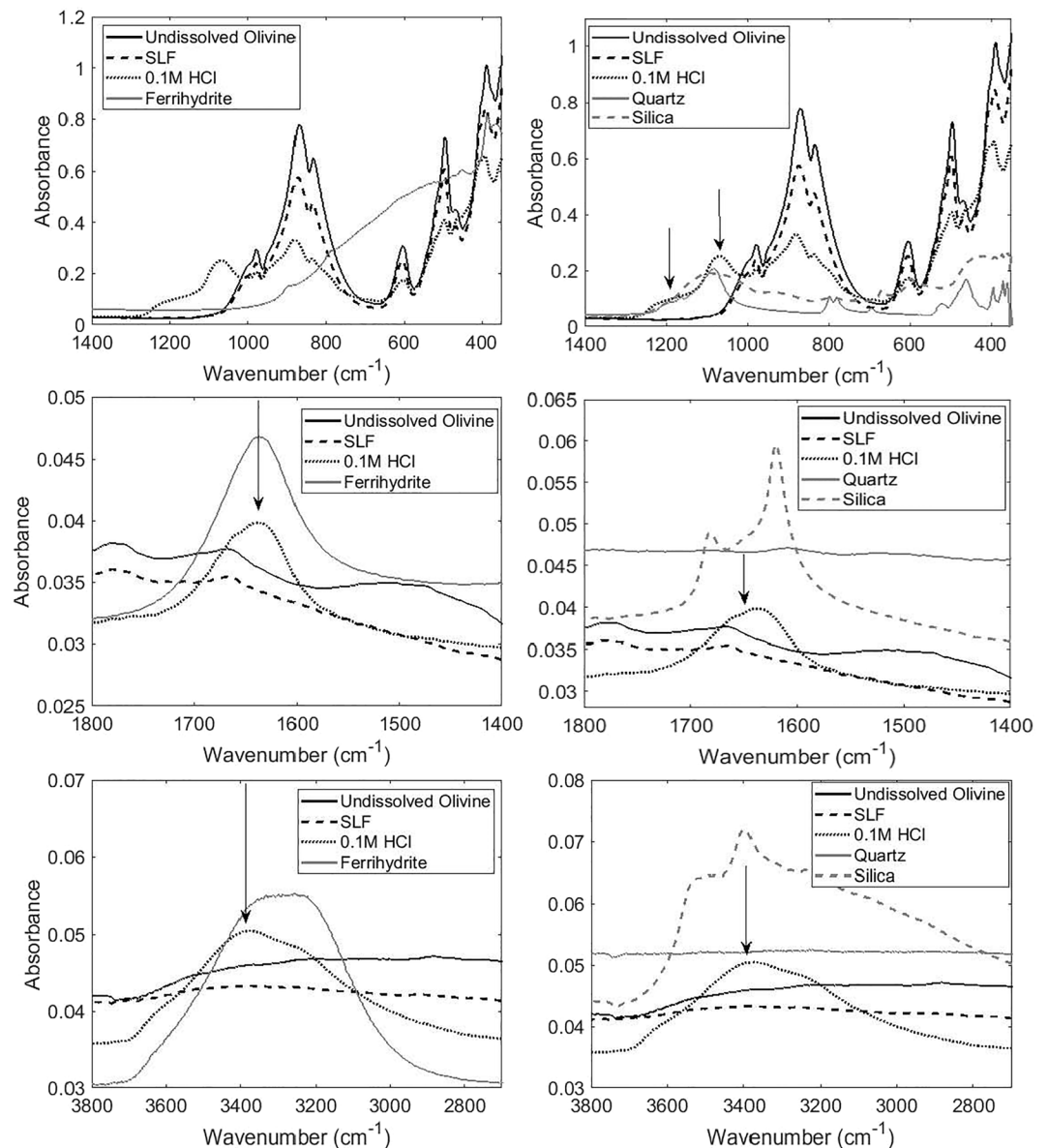


**Figure 12.** ATR-FTIR spectra of olivine dissolved in both 0.1 M HCl and SLF compared to spectra of ferrihydrite (left), quartz/silica (right), and unaltered olivine.

## 4. Discussion

### 4.1. Calculation of Olivine Dissolution Rates

Steady state dissolution rates were calculated using Equation 1:

$$R = \frac{Q(C_{\text{out}} - C_{\text{in}})}{mA_s} \quad (1)$$

where  $Q$  ( $\text{L s}^{-1}$ ) is the reactor flow rate,  $C_{\text{out}}$  (M) is the output concentration of Mg, Si, or Fe,  $C_{\text{in}}$  (M) is the input concentration of Mg, Si, or Fe, which is assumed to be zero,  $m$  (g) is the mass of olivine sample,  $A_s$  ( $\text{m}^2 \text{g}^{-1}$ ) is the surface area of olivine sample, and  $R$  ( $\text{mol m}^{-2} \text{s}^{-1}$ ) is the dissolution rate of the mineral. Dissolution rates were calculated for all three elements in both media (0.1 M HCl and SLF) using concentration data from time periods in the experiments when concentrations varied by less than 10%–15%, which is considered the “steady state” condition. While a mineral dissolution rate can be calculated using Fe, Mg, or Si concentration data, olivine dissolution rates are based on Mg concentration data, as the breaking of the Mg-O bond in olivine is the rate-limiting step during the dissolution reaction (Oelkers et al., 2018).

#### 4.1.1. Dissolution in 0.1 M HCl

We calculated a dissolution rate for olivine for each individual run (1–5, Figure 3) using Equation 1 and the average concentration of Mg during the time period from 0–100 hr (Runs 4 and 5), 0–150 hr (Runs 1 and 3) and 0–300 hr (Run 2), when concentrations varied by <15% and olivine dissolution was stoichiometric (Figure 4). During this time period, pH rose to ~4 and then declined before stabilizing around pH 2, after which steady state dissolution ceased. All individual rates were then averaged and the standard deviation on this mean value were calculated and reported on Table 4.

Using rates calculated from Mg concentration data, our average olivine dissolution rate in HCl is  $6.5 \pm 1.0 \times 10^{-9} \text{ mol m}^{-2} \text{ s}^{-1}$ , which is in good agreement with olivine dissolution rates reported elsewhere (Crundwell, 2014; Pokrovsky & Schott, 2000; Rosso & Rimstidt, 2000; Wogelius & Walther, 1991). Rosso and Rimstidt (2000) performed 28 experiments on the dissolution of olivine having identical composition to ours, yielding 488 individual rate determinations. This large number of rate determinations allowed them to perform multiple linear regressions to determine the pre-exponential factor ( $A$ ), activation energy ( $E_A$ ), and rate dependence on pH ( $n$ ) required to calculate olivine dissolution rates across the pH range 1.8–3.8 and temperature range 25–45°C (their Equation 6). Using their Equation 6, we calculate for 37°C between pH 2 and 4 (the range observed during steady-state dissolution in our experiments) a potential range in olivine dissolution rates of  $2.3 \times 10^{-09}$  to  $2.3 \times 10^{-08} \text{ mol m}^{-2} \text{ s}^{-1}$ ; our experimentally determined dissolution rate falls within this range. The high surface area observed for our reacted olivine samples is likely due to both the dissolution of the olivine crystal structure and the possible precipitation of both an amorphous silica-rich component and ferrihydrite, as shown by SEM, EDX, and IR data (Figures 8c, 10c, and 12).

**Table 4**  
Calculated Steady State Dissolution Rates for Olivine in 0.1 M HCl and SLF in Our Work and Calculated Error Using Error Propagation

Olivine dissolution (SLF)	Average rate ( $\text{mol m}^{-2} \text{s}^{-1}$ )	Average rate error ( $\text{mol m}^{-2} \text{s}^{-1}$ )
Fe	$9.29 \times 10^{-13}$	$1.67 \times 10^{-13}$
Si	$6.33 \times 10^{-12}$	$1.25 \times 10^{-12}$
Mg	$1.54 \times 10^{-11}$	$2.03 \times 10^{-12}$
Olivine dissolution (0.1 M HCl)	Average rate ( $\text{mol m}^{-2} \text{s}^{-1}$ )	Average rate error ( $\text{mol m}^{-2} \text{s}^{-1}$ )
Fe	$6.88 \times 10^{-10}$	$1.08 \times 10^{-10}$
Si	$3.14 \times 10^{-09}$	$5.36 \times 10^{-10}$
Mg	$6.45 \times 10^{-09}$	$9.71 \times 10^{-10}$



#### 4.1.2. Dissolution in SLF

Steady state dissolution was achieved for olivine in SLF at approximately 250–300 hr in Runs 1, 2, 5, and 6. As shown in Figure 5, concentrations varied by less than 15% for this time interval for all elements, and Si/Mg ratios stabilize at a value of  $\sim 1$ . For Runs 3 and 4, Si and Mg concentrations continue to decline across this time interval, indicating that steady state conditions may not have been achieved for these two experiments. Accordingly, we calculated dissolution rates for runs 1, 2, 5, and 6 using the average concentrations measured after 250 hr, and then calculated an average rate from all four experiments as described above (Table 4). Using rates calculated from Mg concentration data, our average olivine dissolution rate in SLF is  $1.5 \pm 0.20 \times 10^{-11} \text{ mol m}^{-2} \text{ s}^{-1}$ , about three orders of magnitude slower compared to olivine dissolved in 0.1 M HCl. During the time interval for which rates were calculated, pH was constant and elevated relative to the inlet fluid pH. It can be concluded that our olivine samples dissolve about 400 times slower in SLF than in 0.1 M HCl. Based on our measured olivine dissolution rates in SLF and assuming a spherical  $1 \mu\text{m}$  diameter olivine particle, a molar volume of  $43.79 \text{ cm}^3 \text{ mol}^{-1}$  (Robie & Bethke, 1962), and Equation 17 in Lasaga (1984), which provides a mathematical formulation for calculating the lifetime of spherical particles, it would take approximately 24 years for a  $1 \mu\text{m}$  diameter particle to completely dissolve in the human lung at our experimentally determined dissolution rate. These results indicate that olivine particles may reside in the lungs for entire human life spans if they are larger than  $1 \mu\text{m}$ . Lunar dust inhalation may lead to severe oxidative damage to both epithelial and endothelial cells, inflammation, etc. These potential adverse effects may lead to the inhibition of the clearance mechanisms responsible for clearing out the lungs of foreign particulate matter. Thus olivine and other mineral dust matter on the Moon may reside for long periods of time in the human lungs. In contrast, a  $1 \mu\text{m}$  diameter olivine particle exposed to 0.1 M HCl, similar in respect to the pH of gastric fluid, would dissolve in less than one month, and would thus likely pass through the human gastrointestinal (GI) tract prior to being completely dissolved, or if unable to be passed from the stomach, would dissolve in a relatively short period of time.

#### 4.1.3. Mineral Precipitation

Given that particulate olivine can reside in the lung for the entire span of a human lifetime and be in contact with a fluid medium including alveolar fluid, it seems reasonable to expect that the ions released from olivine as dissolved constituents might precipitate as low temperature secondary mineral phases, such as minerals commonly observed in chemical weathering reactions, up to approximately  $70^\circ\text{C}$ . This of course depends on how effectively lunar dust components inhibit particle clearance mechanisms via oxidative damage to living cells. While ATR spectra lacked evidence for any secondary precipitates from olivine in SLF, X-ray diffraction evidence exists for possible presence of a secondary precipitate (Figure 11b), combined with an increase in surface area during dissolution in SLF (change from  $3.0$  to  $4.56 \text{ m}^2 \text{ g}^{-1}$ ), indicating that such mineral precipitation reactions may be occurring even in the relatively short time span of our experiments. To further understand what mineral phases might be expected to precipitate as a result of long-term olivine-lung fluid interaction, we entered the measured output solution chemistry from our experiments into PHREEQC v3.5 to determine the saturation state of those fluids with respect to low-temperature secondary minerals. As shown on Table 5, the output solutions from SLF experiments are saturated with respect to a variety of iron oxide phases (ferrihydrite, goethite, hematite); the extremely low dissolved iron concentrations ( $\sim 5\text{--}12 \mu\text{M}$ ) observed in our SLF experiments is consistent with this modeling result and indicates that a secondary Fe-oxide phase likely precipitated in our experiments, though we did not observe any secondary Fe-oxides in our XRD patterns or ATR spectra, likely due to the very slow dissolution rate of olivine in SLF.

PHREEQC also indicates that brucite ( $\text{Mg}(\text{OH})_2$ ), and the magnesium phyllosilicates talc and sepiolite are saturated in our experiments. While these minerals do not exhibit XRD reflections in the same location as the low 2-theta reflection observed in our experimental solids (Figure 11b), the position of that reflection is consistent with the presence of a secondary Mg-phyllosilicate phase such as chrysotile, clinocllore, or chamosite. Minerals such as chrysotile and sepiolite form needle-like crystal structures which can have long term impacts on human health similar to that observed for asbestos (Hardy & Aust, 1995). An identical simulation

**Table 5**  
Modeled Mineral Phases Generated by PHREEQC v3.5 for Both Olivine Dissolved in 0.1 M HCl and SLF

0.1 M HCl	SLF
Goethite	Chrysotile
Hematite	Fe(OH) <sub>3</sub>
Quartz	Goethite
	Hematite
	Sepiolite
	Talc

conducted on the output fluids from the 0.1 M HCl experiments indicate that the iron oxides goethite and hematite are saturated, along with quartz. In our ATR spectra we observe features likely associated with the Fe-oxyhydroxide ferrihydrite, rather than goethite or hematite, which typically form as a result of the dehydration of precursor mineraloids such as ferrihydrite. Saturation with respect to quartz is unsurprising given the high silica concentrations in these solutions, and in fact, the broad amorphous “hump” observed in our XRD patterns from solids from these experiments, SEM-EDS observations, and spectral features in our ATR spectra indicate that instead of quartz, amorphous silica precipitated during experimentation.

#### 4.2. Long-Term OH\* Release in Solution

Olivine in 0.1 M HCl versus SLF both demonstrate different patterns in OH\* generation as shown in Figure 10. Initial incubation of olivine in 0.1 M HCl causes a large burst of OH\* generation followed by a rapid drop in reactivity to zero and below that of olivine in SLF. Olivine in SLF retains its reactivity, albeit in low levels, for 5–6 days before dropping to zero. This is most likely due to the fact that 0.1 M HCl dissolves surficial defects sites approximately 400 times faster relative to SLF. Generation of OH\* will continue longer in the lung fluid but would eventually drop off to zero after a few days as the olivine particle persists in the human lung and continues to dissolve.

#### 4.3. Implications for Human Health

The implications of this work point out that olivine grains do not dissolve readily once inside the human lungs which can lead to a variety of health concerns, especially in the alveolar regions (Fronius et al., 2012; Matthay et al., 2002; Zhu et al., 2001). Based on the dissolution rates for olivine in SLF, we estimate that an olivine particle 1  $\mu\text{m}$  in diameter would take approximately 24 years to completely dissolve in the human lung. Larger particles would take longer to dissolve in the body potentially leading to adverse long-term effects such as silicosis, fibrosis, chronic obstructive pulmonary disease (COPD), and cancer, especially when accounting for precipitated secondary minerals (Hardy & Aust, 1995; Schoonen et al., 2006). It is unknown what effects any precipitated minerals would have on human lungs, but PHREEQC models show that it is possible to precipitate out minerals with fibrous crystal structures and high surface areas which can cause symptoms similar to asbestos exposure. Scar tissue buildup due to abrasion caused by particles can lead to fibrosis. It is important to keep in mind that olivine will continuously dissolve into the solution in the lungs, it does not consider the dissolution times of secondary mineral phases which can have either longer or shorter residence times in the human lungs. A 1  $\mu\text{m}$  chrysotile asbestos particle has a lung residence time of approximately 1 year (Hume & Rimstidt, 1992). When chrysotile dissolves, it eventually leaves behind an amorphous silica component of which a 1  $\mu\text{m}$  particle can take over 400 years to fully dissolve (Rimstidt & Barnes, 1980). A 1  $\mu\text{m}$  diameter particle of talc was determined to dissolve in approximately 8 years at neutral pH and 37°C (Jurinski & Rimstidt, 2001). Any amorphous silica left behind by dissolution of secondary minerals would have residence times many times higher than that of the typical human lifespan. Long term effects of iron-rich silicates may include the oxidation of the nucleotides of DNA and oxidation of lipids (Hardy & Aust, 1995). Astronauts during the Apollo missions were on the lunar surface for no more than a few hours total per mission. Humans working on the lunar surface for multiple days or weeks would have higher chances of being exposed to large quantities of lunar dust particles. The long-term effects of lunar dust exposure are not well known but if they are similar to the long-term effects of asbestos exposure on Earth then lunar explorers could face decades of health concerns if dust mitigation systems are not adequate or fail. Health complications such as lung cancer, mesothelioma, and asbestosis occur about 10–20 years after initial exposure (Ross, 1984). It is uncertain whether lunar dust exposure would lead to this same effect or not. Significantly more studies need to be conducted in order understand lunar dust reactivity, toxicity, and bioaccessibility in biologically relevant aqueous media.

### 5. Conclusions

The residence time of a 1  $\mu\text{m}$  diameter olivine particle in the human lung is estimated to be approximately 24 years. This raises concerns for potential detrimental health impacts of astronauts conducting missions on the lunar surface. Olivine is the third most abundant mineral phase present on the lunar surface and

has the risk of infiltrating the human respiratory systems of future lunar explorers. Particles as large as 10  $\mu\text{m}$  can be trapped in the human respiratory system and olivine particles that size can have residence times longer than the average human lifespan. Short term health effects include DNA damage due to the generation of OH\* but the long-term implications are still not well understood. Precipitation of mineral phases such as chrysotile and sepiolite may cause adverse health implications due to the fibrous crystal structure and high surface areas these minerals have in common with asbestos. More work needs to be done in both understanding the toxicity of olivine dusts and the mitigation of potential side effects. Accidental exposures to lunar dusts containing olivine plus other mineral phases may have longer residence times and may precipitate out other unknown secondary mineral phases. Previous lunar dust toxicology studies were done with Apollo 14 dust which likely exhibits a differing chemical composition to any dust samples present in the lunar south pole region, the area where Artemis III is expected to land. Since south polar samples currently are not available on Earth, studying human health impacts on a mineral-by-mineral basis is the best way forward as the results can then be extrapolated universally across the mineralogically heterogeneous lunar landscape. While lunar dust mitigation efforts are important, it is uncertain how effective these systems will be during the Artemis III mission. Filtration systems had varying success on the Apollo missions. Regardless of the potential efficacy of these new systems, it is important to understand the health impacts of accidental lunar dust exposure in order for future astronauts to be fully prepared and knowledgeable for whatever challenges may arise.

### Conflict of Interest

The authors declare no conflicts of interest relevant to this study.

### Data Availability Statement

The data that support the findings of this study are openly available in Zenodo at <http://doi.org/10.5281/zenodo.4568543>.

### Acknowledgments

This work was supported by the RISE2 node of the NASA Solar System Exploration Research Virtual Institute (SSERVI) under Cooperative Agreements NNA114AB04A and Grant 80NSSC19M0215. The authors would like to thank Jim Quinn who obtained SEM measurements for our mineral samples.

### References

- Angelé-Martínez, C., Goodman, C., & Brumaghim, J. (2014). Metal-mediated DNA damage and cell death: Mechanisms, detection methods, and cellular consequences. *Metalomics*, 6(8), 1358–1381. <https://doi.org/10.1039/c4mt00057a>
- Bastacky, J., Lee, C., Goerke, J., Koushafar, H., Yager, D., Kenaga, L., et al. (1995). Alveolar lining layer is thin and continuous: Low-temperature scanning electron microscopy of rat lung. *Journal of Applied Physiology*, 79(5), 1615–1628. <https://doi.org/10.1152/jap.1995.79.5.1615>
- Bauer, J., Mattson, S. M., & Eastes, W. (1997). *In-vitro acellular method for determining fiber durability in simulated lung fluid*.
- Bos, P. M., Gosens, I., Geraets, L., Delmaar, C., & Cassee, F. R. (2019). Pulmonary toxicity in rats following inhalation exposure to poorly soluble particles: The issue of impaired clearance and the relevance for human health hazard and risk assessment. *Regulatory Toxicology and Pharmacology*, 109, 104498. <https://doi.org/10.1016/j.yrtph.2019.104498>
- Byrne, S., Dyar, M., Besset, E., Breitenfeld, L., Crowley, M., Hoff, C., et al. (2015). Pure mineral separates for mixing experiments to simulate planetary surfaces. In *Paper presented at the Lunar and Planetary Science Conference*.
- Caston, R., Luc, K., Hendrix, D., Hurowitz, J. A., & Demple, B. (2018). Assessing toxicity and nuclear and mitochondrial DNA damage caused by exposure of mammalian cells to Lunar regolith simulants. *Geohealth*, 2(4), 139–148. <https://doi.org/10.1002/2017GH000125>
- Champion, J. A., Walker, A., & Mitragotri, S. (2008). Role of particle size in phagocytosis of polymeric microspheres. *Pharmaceutical Research*, 25(8), 1815–1821. <https://doi.org/10.1007/s11095-008-9562-y>
- Cohn, C. A., Laffers, R., & Schoonen, M. A. (2006). Using yeast RNA as a probe for generation of hydroxyl radicals by earth materials. *Environmental Science & Technology*, 40(8), 2838–2843. <https://doi.org/10.1021/es052301k>
- Colaprete, A., Schultz, P., Heldmann, J., Wooden, D., Shirley, M., Ennico, K., et al. (2010). Detection of water in the LCROSS ejecta plume. *Science*, 330(6003), 463–468. <https://doi.org/10.1126/science.1186986>
- Cooke, N., & Holt, F. (1974). The solubility of some uranium compounds in simulated lung fluid. *Health Physics*, 27(1), 69–77. <https://doi.org/10.1097/00004032-197407000-00009>
- Crane, L. (2019). *Crewed missions to the moon*. Elsevier.
- Crundwell, F. K. (2014). The mechanism of dissolution of forsterite, olivine and minerals of the orthosilicate group. *Hydrometallurgy*, 150, 68–82. <https://doi.org/10.1016/j.hydromet.2014.09.006>
- Dizdaroğlu, M., Rao, G., Halliwell, B., & Gajewski, E. (1991). Damage to the DNA bases in mammalian chromatin by hydrogen peroxide in the presence of ferric and cupric ions. *Archives of Biochemistry and Biophysics*, 285(2), 317–324. [https://doi.org/10.1016/0003-9861\(91\)90366-q](https://doi.org/10.1016/0003-9861(91)90366-q)
- Driscoll, K. E., & Borm, P. J. (2020). Expert workshop on the hazards and risks of poorly soluble low toxicity particles. *Inhalation Toxicology*, 32(2), 53–62. <https://doi.org/10.1080/08958378.2020.1735581>
- Drysdale, M., Bjorklund, K. L., Jamieson, H. E., Weinstein, P., Cook, A., & Watkins, R. T. (2012). Evaluating the respiratory bioaccessibility of nickel in soil through the use of a simulated lung fluid. *Environmental Geochemistry and Health*, 34(2), 279–288. <https://doi.org/10.1007/s10653-011-9435-x>

- Drysdale, M., & Jamieson, H. (2008). *Application of simulated lung fluid analysis to characterize the influence of smelter activity on the respiratory bioaccessibility of nickel-bearing soils in Kalgoorlie, Western Australia.*
- Fronius, M., Clauss, W. G., & Althaus, M. (2012). Why do we have to move fluid to be able to breathe? *Frontiers in Physiology*, 3, 146. <https://doi.org/10.3389/fphys.2012.00146>
- Fubini, B., & Hubbard, A. (2003). Reactive oxygen species (ROS) and reactive nitrogen species (RNS) generation by silica in inflammation and fibrosis. *Free Radical Biology and Medicine*, 34(12), 1507–1516. [https://doi.org/10.1016/s0891-5849\(03\)00149-7](https://doi.org/10.1016/s0891-5849(03)00149-7)
- Gainey, S. R., Hausrath, E. M., Hurowitz, J. A., & Milliken, R. E. (2014). Nontronite dissolution rates and implications for Mars. *Geochimica et Cosmochimica Acta*, 126, 192–211. <https://doi.org/10.1016/j.gca.2013.10.055>
- Gamble, J. F. (1986). Silicate pneumoconiosis. *Occupational Respiratory Diseases DHHS (NIOSH) Publication* (Vol. 86–102, pp. 243–285).
- García-Pérez, J., López-Abente, G., Castelló, A., González-Sánchez, M., & Fernández-Navarro, P. (2015). Cancer mortality in towns in the vicinity of installations for the production of cement, lime, plaster, and magnesium oxide. *Chemosphere*, 128, 103–110. <https://doi.org/10.1016/j.chemosphere.2015.01.020>
- Gilmour, P. S., Beswick, P. H., Brown, D. M., & Donaldson, K. (1995). Detection of surface free radical activity of respirable industrial fibres using supercoiled phi X174 RF1 plasmid DNA. *Carcinogenesis*, 16(12), 2973–2979. <https://doi.org/10.1093/carcin/16.12.2973>
- Hardy, J. A., & Aust, A. E. (1995). Iron in asbestos chemistry and carcinogenicity. *Chemical Reviews*, 95(1), 97–118. <https://doi.org/10.1021/cr00033a005>
- Harrington, A. D., Hylton, S., & Schoonen, M. A. A. (2012). Pyrite-driven reactive oxygen species formation in simulated lung fluid: Implications for coal workers' pneumoconiosis. *Environmental Geochemistry and Health*, 34(4), 527–538. <https://doi.org/10.1007/s10653-011-9438-7>
- Harrington, A. D., Tsirka, S. E., & Schoonen, M. A. A. (2013). Inflammatory stress response in A549 cells as a result of exposure to coal: Evidence for the role of pyrite in coal workers' pneumoconiosis pathogenesis. *Chemosphere*, 93(6), 1216–1221. <https://doi.org/10.1016/j.chemosphere.2013.06.082>
- Heiken, G. H., Vaniman, D. T., & French, B. M. (1991). *Lunar sourcebook: A user's guide to the moon* (pp. 1–736). Cambridge University Press. No individual items are abstracted in this volume.
- Hendrix, D. A., Port, S. T., Hurowitz, J. A., & Schoonen, M. A. (2019). Measurement of OH\* generation by pulverized minerals using Electron Spin Resonance spectroscopy and implications for the reactivity of planetary regolith. *Geohealth*, 3(1), 28–42. <https://doi.org/10.1029/2018gh000175>
- Hickson, C. J., & Juras, S. J. (1986). Sample contamination by grinding. *The Canadian Mineralogist*, 24(3), 585–589.
- Horwell, C. J. (2007). Grain-size analysis of volcanic ash for the rapid assessment of respiratory health hazard. *Journal of Environmental Monitoring*, 9(10), 1107–1115. <https://doi.org/10.1039/B710583P>
- Horwell, C. J., Fenoglio, I., & Fubini, B. (2007). Iron-induced hydroxyl radical generation from basaltic volcanic ash. *Earth and Planetary Science Letters*, 261(3–4), 662–669. <https://doi.org/10.1016/j.epsl.2007.07.032>
- Hume, L. A., & Rimstidt, J. D. (1992). The bi durability of chrysotile asbestos. *American Mineralogist*, 77(9–10), 1125–1128.
- Hurowitz, J. A., McLennan, S., Lindsley, D., & Schoonen, M. (2005). Experimental epithermal alteration of synthetic Los Angeles meteorite: Implications for the origin of Martian soils and identification of hydrothermal sites on Mars. *Journal of Geophysical Research*, 110. <https://doi.org/10.1029/2004JE002391>
- Hurowitz, J. A., Tosca, N. J., McLennan, S. M., & Schoonen, M. A. (2007). Production of hydrogen peroxide in Martian and lunar soils. *Earth and Planetary Science Letters*, 255(1–2), 41–52. <https://doi.org/10.1016/j.epsl.2006.12.004>
- James, J. T., Lam, C., Scully, R. R., Meyers, V. E., & McCoy, J. (2014). *Lunar dust toxicity: Final report*. NASA.
- James, J. T., Lam, C.-W., Santana, P. A., & Scully, R. R. (2013). Estimate of safe human exposure levels for lunar dust based on comparative benchmark dose modeling. *Inhalation Toxicology*, 25(5), 243–256. <https://doi.org/10.3109/08958378.2013.777821>
- Jurinski, J. B., & Rimstidt, J. D. (2001). Bi durability of talc. *American Mineralogist*, 86(4), 392–399. <https://doi.org/10.2138/am-2001-0402>
- Kaur, J., Rickman, D., & Schoonen, M. A. (2016). Reactive Oxygen Species (ROS) generation by lunar simulants. *Acta Astronautica*, 122, 196–208. <https://doi.org/10.1016/j.actaastro.2016.02.002>
- King, E., Rogers, N., Gilchrist, M., Goldschmidt, V., & Nagelschmidt, G. (1945). The effect of olivine on the lungs of rats. *Journal of Pathology and Bacteriology*, 57(4), 488–491. <https://doi.org/10.1002/path.1700570414>
- Klein, S. (2010). The use of biorelevant dissolution media to forecast the in vivo performance of a drug. *The AAPS Journal*, 12(3), 397–406. <https://doi.org/10.1208/s12248-010-9203-3>
- Knudsen, L., & Ochs, M. (2018). The micromechanics of lung alveoli: Structure and function of surfactant and tissue components. *Histochemistry and Cell Biology*, 150(6), 661–676. <https://doi.org/10.1007/s00418-018-1747-9>
- Labotka, T., Kempa, M., White, C., & Papike, J. (1980). The lunar regolith: Comparative petrology of the sampling sites. In *Paper presented at the Lunar and Planetary Science Conference*.
- Lam, C.-W., Scully, R. R., Zhang, Y., Renne, R. A., Hunter, R. L., McCluskey, R. A., et al. (2013). Toxicity of lunar dust assessed in inhalation-exposed rats. *Inhalation Toxicology*, 25(12), 661–678. <https://doi.org/10.3109/08958378.2013.833660>
- Lambrecht, B. N. (2006). Alveolar macrophage in the driver's seat. *Immunity*, 24(4), 366–368. <https://doi.org/10.1016/j.immuni.2006.03.008>
- Lasaga, A. C. (1984). Chemical kinetics of water-rock interactions. *Journal of Geophysical Research: solid earth*, 89(B6), 4009–4025. <https://doi.org/10.1029/JB089iB06p04009>
- Lewis, B. M., Lin, T.-H., Noe, F. E., Hayford-Welsing, E. J., & Flaherty, E. (1959). The measurement of pulmonary diffusing capacity for carbon monoxide by a rebreathing method. *Journal of Clinical Investigation*, 38(11), 2073–2086. <https://doi.org/10.1172/jci103985>
- Li, M., Thompson, K. K., Nissen, J. C., Hendrix, D., Hurowitz, J. A., & Tsirka, S. E. (2019). Lunar soil simulants alter macrophage survival and function. *Journal of Applied Toxicology*, 39(10), 1413–1423. <https://doi.org/10.1002/jat.3827>
- Lindert, J., Perlman, C. E., Parthasarathi, K., & Bhattacharya, J. (2007). Chloride-dependent secretion of alveolar wall liquid determined by optical-sectioning microscopy. *American Journal of Respiratory Cell and Molecular Biology*, 36(6), 688–696. <https://doi.org/10.1165/rcmb.2006-0347OC>
- Linnarsson, D., Carpenter, J., Fubini, B., Gerde, P., Karlsson, L. L., Loftus, D. J., et al. (2012). Toxicity of lunar dust. *Planetary and Space Science*, 74(1), 57–71. <https://doi.org/10.1016/j.pss.2012.05.023>
- Loftus, D., Rask, J., McCrossin, C., & Tranfield, E. (2010). The chemical reactivity of lunar dust: From toxicity to astrobiology. *Earth, Moon, and Planets*, 107(1), 95–105. <https://doi.org/10.1007/s11038-010-9376-x>
- Luce, R. W., Bartlett, R. W., & Parks, G. A. (1972). Dissolution kinetics of magnesium silicates. *Geochimica et Cosmochimica Acta*, 36(1), 35–50. [https://doi.org/10.1016/0016-7037\(72\)90119-6](https://doi.org/10.1016/0016-7037(72)90119-6)
- Matthay, M. A., Folkesson, H. G., & Clerici, C. (2002). Lung epithelial fluid transport and the resolution of pulmonary edema. *Physiological Reviews*, 82(3), 569–600. <https://doi.org/10.1152/physrev.00003.2002>



- McKay, D., Cooper, B., Taylor, L., James, J., Thomas-Keprta, K., Pieters, C., et al. (2015). Physicochemical properties of respirable-size lunar dust. *Acta Astronautica*, 107, 163–176. <https://doi.org/10.1016/j.actaastro.2014.10.032>
- Meyers, V. E., Garcia, H. D., Monds, K., Cooper, B. L., & James, J. T. (2012). Ocular toxicity of authentic lunar dust. *BMC Ophthalmology*, 12(1), 26. <https://doi.org/10.1186/1471-2415-12-26>
- Middleton, E. (1936). Industrial pulmonary disease due to the inhalation of dust. With special reference to silicosis. *Lancet*, 59–64. [https://doi.org/10.1016/S0140-6736\(00\)48130-4](https://doi.org/10.1016/S0140-6736(00)48130-4)
- Ng, A. W., Bidani, A., & Heming, T. A. (2004). Innate host defense of the lung: Effects of lung-lining fluid pH. *Lung*, 182(5), 297–317. <https://doi.org/10.1007/s00408-004-2511-6>
- Nikula, K. J., Avila, K. J., Griffith, W. C., & Mauderly, J. L. (1997). Sites of particle retention and lung tissue responses to chronically inhaled diesel exhaust and coal dust in rats and cynomolgus monkeys. *Environmental Health Perspectives*, 105(5), 1231–1234. <https://doi.org/10.1289/ehp.97105s51231>
- Nikula, K. J., Vallyathan, V., Green, F., & Hahn, F. F. (2001). Influence of exposure concentration or dose on the distribution of particulate material in rat and human lungs. *Environmental Health Perspectives*, 109(4), 311–318. <https://doi.org/10.1289/ehp.01109311>
- Oberdorster, G., Oberdorster, E., & Oberdorster, J. (2005). Nanotoxicology: An emerging discipline evolving from studies of ultrafine particles. *Environmental Health Perspectives*, 113(7), 823–839. <https://doi.org/10.1289/ehp.7339>
- Oelkers, E. H., Declercq, J., Saldi, G. D., Gislason, S. R., & Schott, J. (2018). Olivine dissolution rates: A critical review. *Chemical Geology*, 500, 1–19. <https://doi.org/10.1016/j.chemgeo.2018.10.008>
- Papike, J. J., Simon, S. B., & Laul, J. C. (1982). The lunar regolith: Chemistry, mineralogy, and petrology. *Reviews of Geophysics*, 20(4), 761–826. <https://doi.org/10.1029/RG020i004p00761>
- Park, J., Liu, Y., Kihm, K. D., & Taylor, L. A. (2008). Characterization of lunar dust for toxicological studies. I: Particle size distribution. *Journal of Aerospace Engineering*, 21(4), 266–271. [https://doi.org/10.1061/\(asce\)0893-1321\(2008\)21:4\(266\)](https://doi.org/10.1061/(asce)0893-1321(2008)21:4(266))
- Parkhurst, D. L., & Appelo, C. (2013). *Description of input and examples for PHREEQC version 3: A computer program for speciation, batch-reaction, one-dimensional transport, and inverse geochemical calculations* (pp. 1–497). <https://doi.org/10.3133/tm6A43>
- Pokrovsky, O. S., & Schott, J. (2000). Kinetics and mechanism of forsterite dissolution at 25 degrees C and pH from 1 to 12. *Geochimica et Cosmochimica Acta*, 64(19), 3313–3325. [https://doi.org/10.1016/S0016-7037\(00\)00434-8](https://doi.org/10.1016/S0016-7037(00)00434-8)
- Porter, D. W., Hubbs, A. F., Robinson, V. A., Battelli, L. A., Greskevitch, M., Barger, M., et al. (2002). Comparative pulmonary toxicity of blasting sand and five substitute abrasive blasting agents. *Journal of Toxicology and Environmental Health Part A*, 65(16), 1121–1140. <https://doi.org/10.1080/152873902760125363>
- Portree, D. S. (1997). *Walking to Olympus: An EVA chronology*. NASA History Office, Office of Policy and Plans. NASA Headquarters.
- Pryor, W. (1988). Why is the OH\* the only radical that commonly adds to DNA—Hypothesis—It has a rare combination of high electrophilicity, high thermochemical reactivity, and a mode of production that can occur near DNA. *Free Radical Biology and Medicine*, 4, 219–223. [https://doi.org/10.1016/0891-5849\(88\)90043-3](https://doi.org/10.1016/0891-5849(88)90043-3)
- Rimstidt, J. D., & Barnes, H. (1980). The kinetics of silica-water reactions. *Geochimica et Cosmochimica Acta*, 44(11), 1683–1699. [https://doi.org/10.1016/0016-7037\(80\)90220-3](https://doi.org/10.1016/0016-7037(80)90220-3)
- Robie, R. A., & Bethke, P. M. (1962). *Molar volumes and densities of minerals* (pp. 4–21). United States Department of the Interior Geological Survey.
- Ross, M. (1984). A survey of asbestos-related disease in trades and mining occupations and in factory and mining communities as a means of predicting health risks of nonoccupational exposure to fibrous minerals. In *Definitions for asbestos and other health-related silicates* (pp. 51–104). ASTM International. <https://doi.org/10.1520/STP39138S>
- Rosso, J. J., & Rimstidt, J. D. (2000). A high resolution study of forsterite dissolution rates. *Geochimica et Cosmochimica Acta*, 64(5), 797–811. [https://doi.org/10.1016/S0016-7037\(99\)00354-3](https://doi.org/10.1016/S0016-7037(99)00354-3)
- Santibañez, M., Alguacil, J., de la Hera, M. G., Navarrete-Muñoz, E. M., Llorca, J., Aragonés, N., et al. (2012). Occupational exposures and risk of stomach cancer by histological type. *Occupational and Environmental Medicine*, 69(4), 268–275. <https://doi.org/10.1136/oemed-2011-100071>
- Sato, T., Takeno, M., Honma, K., Yamauchi, H., Saito, Y., Sasaki, T., et al. (2006). Heme oxygenase-1, a potential biomarker of chronic silicosis, attenuates silica-induced lung injury. *American Journal of Respiratory and Critical Care Medicine*, 174(8), 906–914. <https://doi.org/10.1164/rccm.200508-1237OC>
- Scarpelli, E. M. (2003). Physiology of the alveolar surface network. *Comparative Biochemistry and Physiology Part A: Molecular & Integrative Physiology*, 135(1), 39–104. [https://doi.org/10.1016/S1095-6433\(02\)00352-5](https://doi.org/10.1016/S1095-6433(02)00352-5)
- Scheuchenzuber, W. J., Eskew, M. L., & Zarkower, A. (1985). Effects of prolonged inhalation of silica and olivine dusts on immune functions in the mouse. *Environmental Research*, 38(2), 389–399. [https://doi.org/10.1016/0013-9351\(85\)90100-8](https://doi.org/10.1016/0013-9351(85)90100-8)
- Schoonen, M. A. A., Cohn, C. A., Roemer, E., Laffers, R., Simon, S. R., & O'Riordan, T. (2006). Mineral-induced formation of reactive oxygen species. In N. Sahai & M. A. A. Schoonen (Eds.), *Medical mineralogy and geochemistry* (Vol. 64, pp. 179–221). <https://doi.org/10.2138/rmg.2006.64.7>
- Scully, R. R., & Meyers, V. E. (2015). *Risk of adverse health and performance effects of celestial dust exposure*. NASA.
- Sloniewsky, D. E., Ridge, K. M., Adir, Y., Fries, F. P., Briva, A., Sznajder, J. I., & Sporn, P. H. (2004). Leukotriene D4 activates alveolar epithelial Na, K-ATPase and increases alveolar fluid clearance. *American Journal of Respiratory and Critical Care Medicine*, 169(3), 407–412. <https://doi.org/10.1164/rccm.200304-472OC>
- Tomašek, I., Damby, D. E., Stewart, C., Horwell, C. J., Plumlee, G., Ottley, C. J., et al. (2021). Development of a simulated lung fluid leaching method to assess the release of potentially toxic elements from volcanic ash. *Chemosphere*, 278, 130303. <https://doi.org/10.1016/j.chemosphere.2021.130303>
- Turci, F., Corazzari, I., Alberto, G., Martra, G., & Fubini, B. (2015). Free-radical chemistry as a means to evaluate lunar dust health hazard in view of future missions to the moon. *Astrobiology*, 15(5), 371–380. <https://doi.org/10.1089/ast.2014.1216>
- Turci, F., Ghibaudi, E., Colonna, M., Boscolo, B., Fenoglio, I., & Fubini, B. (2010). An integrated approach to the study of the interaction between proteins and nanoparticles. *Langmuir*, 26(11), 8336–8346. <https://doi.org/10.1021/la904758j>
- Vallyathan, V., Leonard, S., Kuppusamy, P., Pack, D., Chzhnan, M., Sanders, S. P., & Zweir, J. L. (1997). Oxidative stress in silicosis: Evidence for the enhanced clearance of free radicals from whole lungs. *Molecular and Cellular Biochemistry*, 168(1–2), 125–132. <https://doi.org/10.1023/a:1006850920080>
- Vallyathan, V., Mega, J. F., Shi, X. L., & Dalal, N. S. (1992). Enhanced generation of free-radicals from phagocytes induced by mineral dusts. *American Journal of Respiratory Cell and Molecular Biology*, 6(4), 404–413. <https://doi.org/10.1165/ajrcmb/6.4.404>
- Von Sonntag, C., Glass, W., & Varma, M. (1991). In W. A. Glass, & M. N. Varma (Eds.), *Physical and chemical mechanisms in molecular radiation biology* (Vol. 58, pp. 231–287). Plenum Press.

- Wallace, W. T., Phillips, C. J., Jeevarajan, A. S., Chen, B., & Taylor, L. A. (2010). Nanophase iron-enhanced chemical reactivity of ground lunar soil. *Earth and Planetary Science Letters*, 295(3–4), 571–577. <https://doi.org/10.1016/j.epsl.2010.04.042>
- Wallace, W. T., Taylor, L. A., Liu, Y., Cooper, B. L., McKay, D. S., Chen, B., & Jeevarajan, A. S. (2009). Lunar dust and lunar simulant activation and monitoring. *Meteoritics & Planetary Science*, 44(7), 961–970. <https://doi.org/10.1111/j.1945-5100.2009.tb00781.x>
- White, A. F., & Brantley, S. L. (1995). *Chemical weathering rates of silicate minerals* (Vol. 31). Mineralogical Society of America.
- Wiseman, C. L., & Zereini, F. (2014). Characterizing metal(loid) solubility in airborne PM<sub>10</sub>, PM<sub>2.5</sub> and PM<sub>1</sub> in Frankfurt, Germany using simulated lung fluids. *Atmospheric Environment*, 89, 282–289. <https://doi.org/10.1016/j.atmosenv.2014.02.055>
- Wogelius, R. A., & Walther, J. V. (1991). Olivine dissolution at 25°C: Effects of pH, CO<sub>2</sub>, and organic-acids. *Geochimica et Cosmochimica Acta*, 55(4), 943–954. [https://doi.org/10.1016/0016-7037\(91\)90153-v](https://doi.org/10.1016/0016-7037(91)90153-v)
- Xu, C., Zhang, M., Chen, W., Jiang, L., Chen, C., & Qin, J. (2020). Assessment of air pollutant PM<sub>2.5</sub> pulmonary exposure using a 3D lung-on-chip model. *ACS Biomaterials Science & Engineering*, 6(5), 3081–3090. <https://doi.org/10.1021/acsbmaterials.0c00221>
- Zhu, S., Ware, L. B., Geiser, T., Matthay, M. A., & Matalon, S. (2001). Increased levels of nitrate and surfactant protein a nitration in the pulmonary edema fluid of patients with acute lung injury. *American Journal of Respiratory and Critical Care Medicine*, 163(1), 166–172. <https://doi.org/10.1164/ajrccm.163.1.2005068>